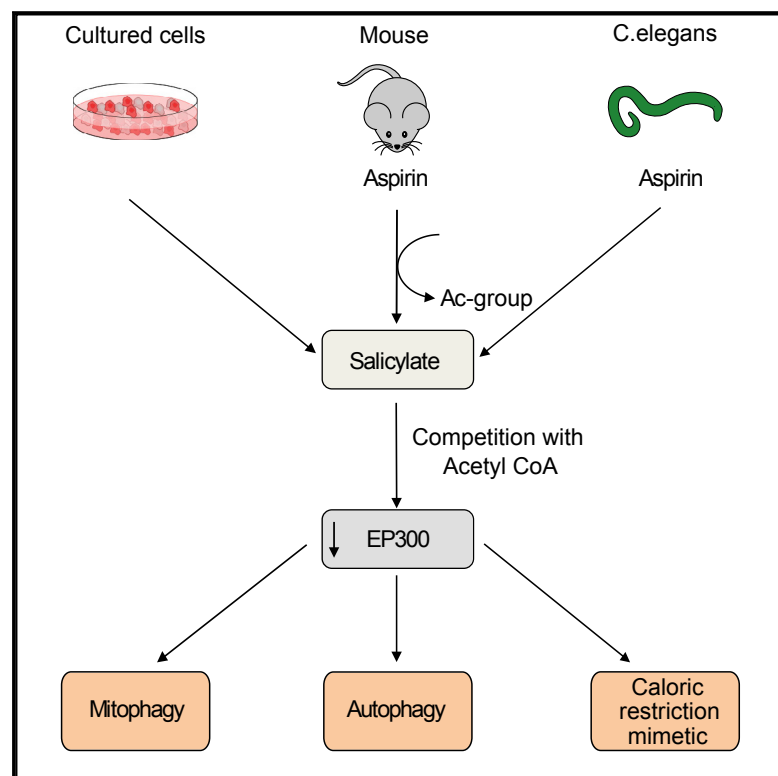# Aspirin Recapitulates Features of Caloric Restriction

Graphical Abstract

Authors

Federico Pietrocola, Francesca Castoldi, Maria Markaki, ..., Junichi Sadoshima, Nektarios Tavernarakis, Guido Kroemer

Correspondence

kroemer@orange.fr

In Brief

Pietrocola et al. show that the inhibition of the acetyltransferase EP300 is determinant for the autophagy-inducing effect of aspirin and its active metabolite salicylate. As a proof of the evolutionarily conserved nature of this mechanism, the authors demonstrate that aspirin triggers protective autophagy in mice and in the nematode *C. elegans*.

Highlights

- The aspirin metabolite, salicylate, competitively inhibits EP300 acetyltransferase

- EP300 inhibition is epistatic to autophagy induction by salicylate

- Aspirin triggers cardioprotective mitophagy in mice and nematodes

CellPress

Aspirin Recapitulates Features
of Caloric Restriction

Federico Pietrocola,[1,2,3,4,5,6,24] Francesca Castoldi,[1,2,3,4,5,6,7,8,24] Maria Markaki,[9,24] Sylvie Lachkar,[1,2,3,4,5,6]
Guo Chen,[1,2,3,4,5,6] David P. Enot,[5] Sylvere Durand,[5] Noelie Bossut,[5] Mingming Tong,[10] Shoaib A. Malik,[1,2,3,4,5,6,11]
Friedemann Loos,[1,2,3,4,5,6] Nicolas Dupont,[4,12,13,14] Guillermo Mariño,[15,16] Nejma Abdelkader,[17] Frank Madeo,[18,19]
Maria Chiara Maiuri,[1,2,3,4,5,6] Romano Kroemer,[20] Patrice Codogno,[4,12,13,14] Junichi Sadoshima,[10]
Nektarios Tavernarakis,[9,21,25] and Guido Kroemer[1,2,3,4,5,6,22,23,25,26,*]

[1]Gustave Roussy Cancer Campus, Villejuif, France
[2]INSERM, U1138, Paris, France
[3]Equipe 11 labellisée par la Ligue Nationale contre le Cancer, Centre de Recherche des Cordeliers, Paris, France
[4]Université Paris Descartes/Paris V, Sorbonne Paris Cité, Paris, France
[5]Metabolomics and Cell Biology Platforms, Gustave Roussy Cancer Campus, Villejuif, France
[6]Université Pierre et Marie Curie, Paris, France
[7]Université Paris-Sud/Paris XI, Faculté de Médecine, Kremlin-Bicêtre, France, Paris, France
[8]Sotio a.c., Prague, Czech Republic
[9]Institute of Molecular Biology and Biotechnology, Foundation for Research and Technology-Hellas, Heraklion 70013, Crete, Greece
[10]Department of Cell Biology and Molecular Medicine, Rutgers–New Jersey Medical School, Newark, NJ, USA
[11]Department of Biochemistry, Sargodha Medical College, Sargodha, Pakistan
[12]Institut Necker-Enfants Malades (INEM), Paris, France
[13]INSERM, U1151, Paris, France
[14]CNRS, UMR8253, Paris, France
[15]Departamento de Biología Fundamental, Universidad de Oviedo, Fundación para la Investigación Sanitaria del Principado de Asturias
(FINBA), Oviedo, Spain
[16]Instituto de Investigación Sanitaria del Principado de Asturias (IISPA), Oviedo, Spain
[17]Scientific Computing, LGCR, Sanofi R&D, 94403 Vitry-sur-Seine, France
[18]Institute of Molecular Biosciences, NAWI Graz, University of Graz, Humboldtstraße 50, 8010 Graz, Austria
[19]BioTechMed-Graz, Humboldtstraße 50, 8010 Graz, Austria
[20]Structure Design & Informatics, LGCR, Sanofi R&D, 94403 Vitry-sur-Seine, France
[21]Department of Basic Sciences, Faculty of Medicine, University of Crete, Heraklion 70013, Crete, Greece
[22]Pôle de Biologie, Hôpital Européen Georges Pompidou, AP-HP, Paris, France
[23]Karolinska Institute, Department of Women's and Children's Health, Karolinska University Hospital, Stockholm, Sweden
[24]These authors contributed equally
[25]Senior author
[26]Lead Contact
*Correspondence: kroemer@orange.fr
https://doi.org/10.1016/j.celrep.2018.02.024

SUMMARY

The age-associated deterioration in cellular and organismal functions associates with dysregulation of nutrient-sensing pathways and disabled autophagy. The reactivation of autophagic flux may prevent or ameliorate age-related metabolic dysfunctions. Non-toxic compounds endowed with the capacity to reduce the overall levels of protein acetylation and to induce autophagy have been categorized as caloric restriction mimetics (CRMs). Here, we show that aspirin or its active metabolite salicylate induce autophagy by virtue of their capacity to inhibit the acetyltransferase activity of EP300. While salicylate readily stimulates autophagic flux in control cells, it fails to further increase autophagy levels in EP300-deficient cells, as well as in cells in which endogenous EP300 has been replaced by salicylate-resistant EP300 mutants. Accordingly, the pro- autophagic activity of aspirin and salicylate on the nematode *Caenorhabditis elegans* is lost when the expression of the EP300 ortholog *cpb-1* is reduced. Altogether, these findings identify aspirin as an evolutionary conserved CRM.

INTRODUCTION

Macroautophagy (hereafter referred to as autophagy) acts as a homeostatic pathway at both the cellular and organismal levels (Mizushima and Komatsu, 2011). The finely tuned execution of this multistep process (ensured by the coordinated activity of specifically committed Atg proteins) eventually culminates in the formation of a double-membrane organelle, the autophagosome, in which bulk portions of the cytoplasm or specific organelles are engulfed prior to their lysosomal hydrolase-mediated degradation (He and Klionsky, 2009). Autophagy may be considered as one of the major anti-aging mechanisms because it assures recycling (and hence rejuvenation) of damaged cytoplasmic components, including entire organelles such as

mitochondria (Pan et al., 2013; Rubinsztein et al., 2011; Sun et al., 2016). Manipulations aiming at restoring or inducing autophagy can reduce the incidence of age-related disease and extend health span and lifespan (López-Otín et al., 2016). The nature of these interventions can be nutritional (i.e., fasting or caloric restriction) (Heilbronn and Ravussin, 2003; Longo and Mattson, 2014), behavioral (i.e., physical activity) (He et al., 2012), or pharmacological. Thus, mTORC1 inhibition by rapalogs (Lamming et al., 2013), activation of sirtuin-1 (SIRT1) with resveratrol (Wood et al., 2004), and supplementation of the natural polyamine spermidine (Eisenberg et al., 2009) extend lifespan in various model organisms in an autophagy-dependent manner (López-Otín et al., 2016). Importantly, overexpression of the autophagy essential gene Atg5 is sufficient to expand lifespan in mice (Pyo et al., 2013), indicating that autophagy is not only necessary but even sufficient to enhance longevity.

Culture of cells in nutrient-free conditions, as well as fasting regimens, leads to a reduction in the global levels of protein acetylation (Eisenberg et al., 2014; Mariño et al., 2014). Reduced acetylation may be explained by the diminution in the activity of nuclear and cytoplasmic lysine-acetyltransferases (KAT) secondary to a decrease in the nucleocytosolic levels of acetyl coenzyme A (CoA), which is the sole donor of acetyl groups (Pietrocola et al., 2015a). As a consequence, blockade of acetyl CoA biosynthesis has the same functional consequence as inhibition of acetyltransferases or activation of the deacetylase activity of sirtuins (Madeo et al., 2014) insofar that it triggers autophagy (Mariño et al., 2014). Chemically unrelated agents, including anacardic acid, hydroxycitrate, resveratrol, and spermidine (Pietrocola et al., 2015b), share the capacity to reduce protein acetylation and have been classified as caloric restriction mimetics (CRMs). CRMs such as spermidine have widespread anti-aging effects (Eisenberg et al., 2016; Pietrocola et al., 2016).

One of the major acetyltransferases that senses cytosolic acetyl CoA levels is adenovirus early region 1A (E1A)-binding protein p300, EP300, which also acts as a master repressor of autophagy (Madeo et al., 2014). Of note, the autophagy inducer spermidine competes with acetyl CoA for binding to the catalytic site of EP300 and, therefore, limits its activity (Morselli et al., 2011; Pietrocola et al., 2015b). Recently, aspirin has been shown to inhibit the enzymatic activity of EP300 as well (Shirakawa et al., 2016). Aspirin (acetylsalicylate), the pro drug of salicylate (which is rapidly formed in vivo through the action of blood and tissue acetylsalicylate hydrolases) (Ali and Kaur, 1983), is probably the pharmacological agent that has the most pleiotropic effects on human health, as it has broad anti-arteriosclerotic and cancer-preventive effects (Baron et al., 2003; Ogawa et al., 2008; Sandler et al., 2003). Beyond its inhibitory action on cyclooxygenases, resulting in the inhibition of prostaglandin synthesis, aspirin affects multiple signal transduction pathways. For example, aspirin reportedly inhibits the activation of the pro-inflammatory transcription factor nuclear factor kappa light-chain enhancer of activated B cell (NF-κB) (Kopp and Ghosh, 1994), and it directly activates the nutrient sensor protein kinase AMP activated (PRKAA1), better known as AMPK (Hawley et al., 2012).

Here we addressed the question as to whether aspirin might have a broad autophagy-inducing effect and whether this effect might be explained by EP300 inhibition. We demonstrate that aspirin fails to modulate autophagic flux in cells lacking EP300 or cells in which EP300 has been engineered to avoid aspirin binding to the acetyl CoA-binding pocket of the enzyme. As a confirmation of the evolutionarily conserved nature of this process, we demonstrate that aspirin failed to further induce autophagy in Caenorhabditis elegans strains deficient for the EP300 homolog CBP-1 or the essential autophagy gene products ATG7 and BEC-1.
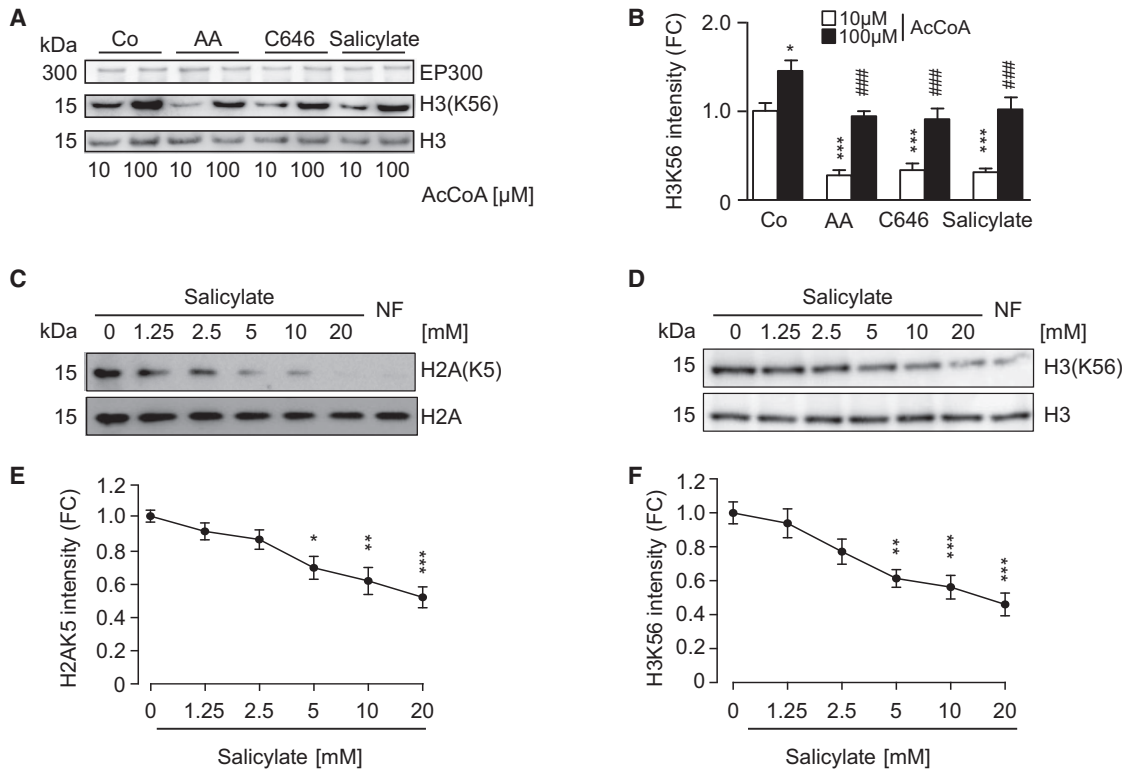
RESULTS

Salicylate Inhibits the Acetyltransferase Activity of EP300

Anacardic acid (AA, also known as 6-pentadecylsalicylic acid) represents the prototypical inhibitor of acetyltransferases from the EP300/PCAF family. In a competitive interaction, the salicylate group of AA displaces the pyrophosphate group of CoA from the KAT domain of EP300 (Ghizzoni et al., 2010). We investigated the possibility that the active aspirin metabolite salicylate itself would inhibit EP300 acetyltransferase activity via a similar mechanism as AA. In a cell-free-based assay, salicylate inhibited the enzymatic activity of recombinant EP300 protein, resulting in reduced acetylation of its natural substrate histone H3 on lysine 56 (H3K56) (Figures 1A and 1B). Importantly, the inhibition of EP300 activity by salicylate was comparable to that of AA or the synthetic EP300 inhibitor C646 (Figures 1A and 1B). This inhibitory effect was achieved at a physiological concentration of acetyl CoA (AcCoA), but it was attenuated by high-dose AcCoA, in line with the idea that it occurred through a competitive mechanism (Figures 1A and 1B), as recently proposed (Shirakawa et al., 2016). Consistently, the administration of salicylate to two different cultured cell lines inhibited the EP300-mediated acetylation of histone 2A (H2AK5) (Figures 1C and 1E) and H3K56 (Figures 1D and 1F) in a dose-dependent manner. Altogether, these data support the hypothesis that salicylate acts as a direct competitive inhibitor of EP300.

Salicylate-Induced Autophagy Depends on EP300 Inhibition

Owing to its ability to directly acetylate key autophagic machinery components, such as Atg5, Atg7, LC3 (Lee and Finkel, 2009), and BECN1 (Sun et al., 2015), EP300 can transduce AcCoA availability into autophagy inhibition. Based on these findings, we determined whether salicylate would induce autophagy through an EP300-dependent mechanism. U2OS cells stably transfected with a fusion protein of GFP and microtubule-associated proteins 1A/1B light chain 3B (GFP-LC3) manifested the formation of cytoplasmic GFP-LC3 puncta upon treatment with salicylate (Figure 2A). Importantly, the increase in number of GFP-LC3 dots was even more prominent when autophagosome-lysosome fusion was impaired by treatment with bafilomycin A1 (BafA1), indicating that salicylate induced autophagic flux (Figure 2A; Table S1). Consistently, human colorectal cancer HCT116 cells treated with two different doses of sodium salicylate exhibited enhanced lipidation of LC3 (as indicated by an increase in its electrophoretic mobility), both in the presence and in the absence of a lysosomal inhibitor (Figure 2B; Table S1).

Figure 1. Salicylate Inhibits EP300 Acetyltransferase by Competing with AcCoA

(A and B) Direct inhibition of EP300 acetyltransferase activity by salicylate. Recombinant EP300 protein was incubated with its substrate histone H3 in the presence of AcCoA, salicylate (5 mM), anacardic acid (AA, 50 μM), or C646 (10 μM), followed by immunoblotting to detect H3 acetylation on lysine 56 (A) and quantification (B) of 4 independent experiments (means ± SEM; *p < 0.05 and ***p < 0.001, one-way ANOVA compared to 10 μM AcCoA control group; ###p < 0.001, one-way ANOVA compared to 100 μM AcCoA; FC, fold change).

(C and D) Salicylate inhibits EP300 activity toward its natural substrates. Human colorectal cancer HCT116 (C) and human osteosarcoma U2OS cells (D) were incubated for 16 hr with the indicated concentration of sodium salicylate and subjected to immunoblotting to evaluate H2A acetylation on lysine 5 (C) and H3 acetylation on lysine 56 (D) (quantified in E and F). Nutrient-free (NF) medium was used as a negative control of acetylation. Representative images of one experiment are shown.
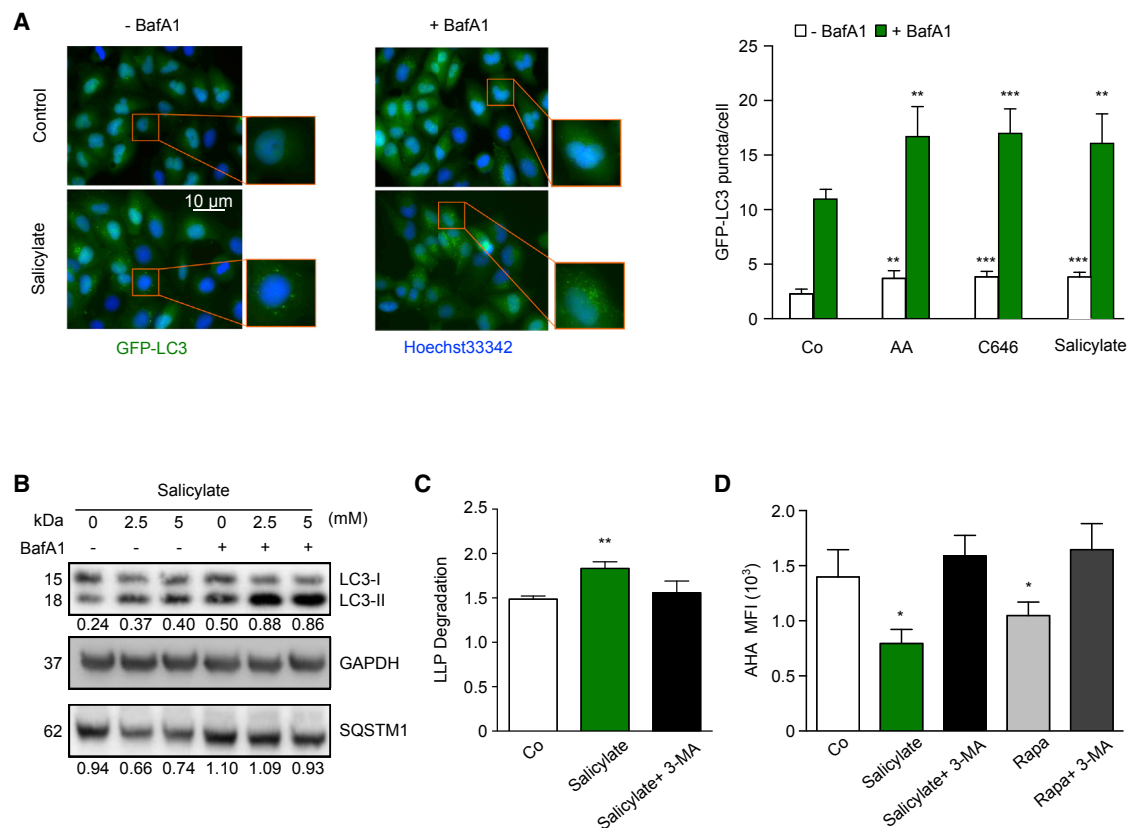
(E and F) Quantification of data depicted in (C) and (D) (means ± SEM; *p < 0.05, **p < 0.01, and ***p < 0.001, one-way ANOVA compared to control group).

In line with the observation that salicylate bona fide promotes autophagic flux, the addition of this compound to cell cultures caused a diminution in the global levels of sequestosome-1 (SQSTM1/p62) (Figure 2B; Table S1) (Klionsky et al., 2016).

In addition, salicylate promoted the autophagy-dependent degradation of long-lived protein, as detected by assessing protein turnover in cells in which proteins were labeled radioactively with [14C]-valine (Bauvy et al., 2009; Dupont et al., 2017) (Figure 2C). Very similar results were obtained when protein turnover was measured after pulse-labeling cells by means of the amino acid analog L-azidohomoalanine (L-AHA), yielding azido-modified proteins that could be visualized by chemoselective ligation with a fluorescent alkyne probe (Wang et al., 2017) (Figure 2D). Importantly, the enhanced protein turnover elicited by salicylate treatment was reversed by the simultaneous addition of the autophagy inhibitor 3-methyladenine to the cell cultures (3-MA), further strengthening the notion that salicylate stimulates autophagic flux (Figures 2C and 2D). Salicylate uptake by cells is mediated by sodium monocarboxylate transporters (Ganapathy

et al., 2008), and cell line-dependent differences in the expression of these carriers may be at the origin of the relatively delayed action of this compound on autophagy and EP300 inhibition. We hence assessed autophagy induction upon short-term treatment with growing concentrations of the cell-permeable salicylate ester ethyl-salicylate. This agent rapidly induced autophagic flux as it inhibited EP300 acetyltransferase activity (Figures S1A–S1C; Table S1).

Incubation of cells with salicylate inhibited the activity of mTORC1 complex (as monitored by the decreased phosphorylation of mTORC1 substrate ribosomal protein S6 kinase beta-1 RPS6KB1, also known as p70[S6K]) and stimulated PRKAA function (as indicated by its increased phosphorylation on Thr 172 by upstream kinases) (Figure S1D; Table S1). This event might be sufficient for triggering autophagy, because PRKAA can directly phosphorylate at least two pro-autophagic proteins, namely, the unc-51-like autophagy-activating kinase 1 (ULK1) (Egan et al., 2011; Kim et al., 2011) and BECN1 (Kim and Guan, 2013). However, the pro-autophagic effect of salicylate

Figure 2. Aspirin Stimulates Autophagic Flux in Cultured Cells

(A and B) *In vitro* effects of the aspirin metabolite salicylate.

(A) U2OS cells expressing GFP-LC3 were treated with salicylate (5 mM), anacardic acid (AA, 50 μM), or C646 (10 μM) in the presence or absence of the lysosomal inhibitor bafilomycin A1 (Baf A1), followed by quantitation of GFP-LC3-positive puncta. Representative images (left panel) and quantitation (right panel) of the number of GFP-LC3 puncta per cell are depicted (**p < 0.01 and ***p < 0.001, unpaired t test compared with respective control condition). Data represent means ± SD from one representative experiment (n = 3).

(B) HCT116 cells were incubated for 16 hr in the presence of growing concentrations of salicylate. Representative immunoblots of 4 independent experiments show the LC3I-to-LC3II conversion (in the presence or absence of BafA1) and depletion of SQSTM1/p62.

(C and D) Analysis of autophagy-dependent long-lived protein (LLP) degradation upon treatment with salicylate.

(C) 3-methyladenine (3-MA)-sensitive degradation of [^{14}C]-valine-labeled long-lived proteins was determined in HCT116 cells upon treatment with salicylate. Values indicate means ± SD from one representative experiment (n = 3; **p < 0.01, unpaired t test compared to control condition).
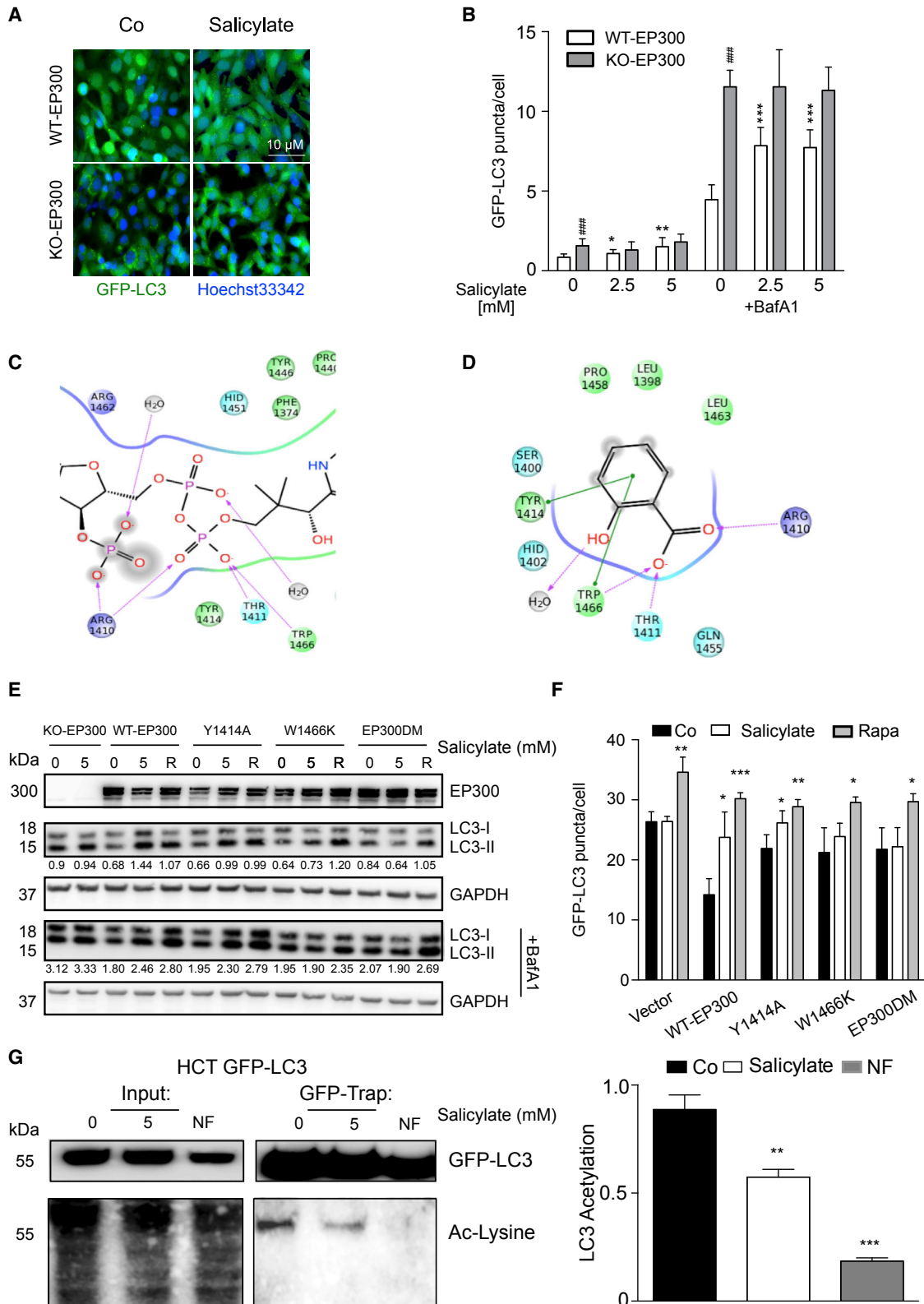
(D) Autophagy-mediated degradation of L-azidohomoalanine (L-AHA)-labeled proteins was assessed in U2OS cells after treatment with salicylate or Rapamycin (Rapa) in the presence or absence of 3-methyladenine. Maximum fluorescence intensity (MFI) values represent means ± SD from one representative experiment (n = 3; *p < 0.05, unpaired t test compared to Co group).

was still observable when the expression of PRKAA α1 subunit was attenuated by transfection of specific small interfering RNAs (siRNAs) (Figures S1E and S1F; Table S1). In accord with previous findings (Din et al., 2012), salicylate still could induce autophagy in mouse embryonic fibroblasts (MEFs) lacking both the α1 and α2 PRKAA subunits (genotype *PRKAAα1$^{-/-}$ PRKAAα2$^{-/-}$*) (Figure S1G; Table S1).

Next, we investigated whether modulation of EP300 activity would be responsible for the pro-autophagic activity of this compound. Epistatic analyses indicated that salicylate was unable to further increase autophagic flux in conditions of EP300 knockout (Figures 3A and 3B; Figure S2A; Table S1) or knockdown (Figure S2B; Table S1), suggesting that it stimulates autophagy through EP300 inhibition. In contrast, rapamycin was able to stimulate autophagy in conditions of EP300 depletion (Figure S2C).

Interestingly, EP300-knockout cells failed to exhibit differences in PRKAA activation levels or upon salicylate treatment when compared to their wild-type (WT) counterparts, suggesting that these pathways act independently of each other (Figure S2D).

Molecular modeling using the bi-substrate inhibitor Lys-CoA (Bowers et al., 2010) docking site of EP300 (Figure 3C) suggested that the introduction of two point mutations would be compatible with AcCoA binding yet prevent salicylate to access the catalytic site (Figure 3D). The knockout (KO)-EP300 HCT116 cells transfected with WT EP300 responded to salicylate by increasing LC3 lipidation (Figure 3E) or generation of LC3 puncta (Figure 3F). In contrast, replacement of endogenous EP300 by the EP300 Y1414A/W1466K double mutant (DM) was unable to restore autophagy induction by salicylate, whereas single W1466K mutation partially impaired autophagic flux (Figures

A

Co   Salicylate

WT-EP300

KO-EP300

GFP-LC3   Hoechst33342

10 μM

B

GFP-LC3 puncta/cell

☐ WT-EP300
▧ KO-EP300

Salicylate [mM]   0   2.5   5   0   2.5   5
+BafA1

C

D

E

	KO-EP300		WT-EP300			Y1414A			W1466K			EP300DM			
Salicylate (mM)	0	5	0	5	R	0	5	R	0	5	R	0	5	R	

kDa

300   EP300

18
15   LC3-I
        LC3-II

0.9 0.94 0.68 1.44 1.07 0.66 0.99 0.99 0.64 0.73 1.20 0.84 0.64 1.05

37   GAPDH

18
15   LC3-I
        LC3-II   +BafA1

3.12 3.33 1.80 2.46 2.80 1.95 2.30 2.79 1.95 1.90 2.35 2.07 1.90 2.69

37   GAPDH

F

GFP-LC3 puncta/cell

■ Co ☐ Salicylate ▧ Rapa

Vector   WT-EP300   Y1414A   W1466K   EP300DM

G

HCT GFP-LC3

Input: GFP-Trap:
kDa   0   5   NF   0   5   NF   Salicylate (mM)

55   GFP-LC3

55   Ac-Lysine

LC3 Acetylation

■ Co ☐ Salicylate ▧ NF

(legend on next page)

3E and 3F). In line with the prediction of the molecular model, the double-mutated form of EP300 was still able to acetylate its specific substrates (and hence to transfer the acetyl moiety of AcCoA on protein), contrasting with its inability to functionally interact with salicylate (Figure S2E).

As a master repressor of the autophagic pathway, EP300 mediates the acetylation of several components of autophagic machinery, including that of LC3 (Huang et al., 2015; Sebti et al., 2014). Indeed, LC3 was deacetylated upon salicylate treatment (Figure 3G), further suggesting that salicylate-induced autophagy occurred through EP300 inhibition.

Injection of aspirin into mice induced signs of autophagy *in vivo* in various organs, including heart (Figure 4A; Figures S3A–S3F) and liver (Figure 4B; Figures S4A–S4F), as suggested by LC3 lipidation, SQSTM1/p62 degradation, and reduction in RPS6KB1 phosphorylation (statistically significant in the heart and with a trend in the liver). These changes were detectable as early as 1 hr post-injection of salicylate, and they were paralleled by a transient inhibition of EP300 activity, as indicated by the reduced acetylation of its natural substrate H3K56 (Figures 4A and 4B). However, the phosphorylation of PRKAA and that of its substrate ACACA occurred at later time points (starting at 6 hr), suggesting that PRKAA activation is unlikely to be involved in the early phase of autophagy induction by aspirin. However, these results do not exclude that PRKAA intervenes in later aspirin effects, which involve complex physiological changes, including non-cell-autonomous signals (Heintz et al., 2017). Importantly, the pro-autophagic effect of salicylate was observed even when the degradation of lysosomal content was inhibited by the injection of leupeptin 2 hr before sacrifice, thus corroborating the evidence that aspirin stimulates autophagic flux in the heart (Figure 4C; Figure S3G) and in the liver (Figure 4D; Figure S4G).

Next we assessed the effect of protracted oral administration of aspirin (2 weeks) on cardiac autophagy in transgenic mice overexpressing the tandem construct GFP-RFP-LC3 in cardiomyocytes (Eisenberg et al., 2016; Hariharan et al., 2011). Aspirin treatment resulted in an increase in the number of red/green fluorescent (autophagosomes) and red fluorescent puncta (autolysosomes), suggestive of autophagy induction in the heart

(Figure 4E). This aspirin-triggered increase in LC3 puncta also occurred in mice treated with chloroquine, further supporting the idea that aspirin indeed stimulated autophagic flux *in vivo* (Figure 4E). Aspirin also potently stimulated one particular type of organelle-specific autophagy, mitophagy (Shirakabe et al., 2016b), in the heart, as monitored by means of a transgene-encoded biosensor, mito-Keima (mt-Keima) (Katayama et al., 2011; Shirakabe et al., 2016a), a mitochondrion-targeted protein that undergoes a pH-dependent excitation shift when it localizes in the acidic lysosomal compartment (Figure 4F).

Aspirin induced LC3 lipidation and SQSTM1 degradation in most organs that we investigated and in particular in heart (Figure 4A), liver (Figure 4B), muscle (Figure S5A), and colon (Figure S5E), but not in brain (Figure S5I) and kidney (Figure S6D). It is known that, when orally administered to healthy human volunteers (Cerletti et al., 1984) or rodents (Higgs et al., 1987), aspirin is rapidly converted into its active metabolites, in particular salicylate, which peaks around 20–30 min in the plasma. However, aspirin metabolism has not been extensively studied by modern metabolomics methods. At 1 hr after intraperitoneal administration of aspirin, significant changes in the metabolome of several organs, including heart (Figure 5A; Table S2), liver (Figure 5D; Table S2), skeletal muscle (Figure S5B; Table S2), colon (Figure S5F; Table S2), brain (Figure S5J; Table S2), plasma (Figure S6A; Table S2), and kidney (Figure S6E; Table S2) occurred, as monitored by mass spectrometry. More importantly, we assessed the presence of peaks indicating the formation of aspirin metabolites in these organs after administering either unlabeled aspirin or [^{13}C]-labeled aspirin, while searching for molecular entities that differ in their mass by exactly 1 Da (Figures 5B and 5E; Figures S5C, S5G, S5K, S6B, and S6F). Several among these unidentified molecular entities were at least as abundant as salicylate (Figures 5C and 5F; Figures S5D, S5H, S5L, S6C, and S6G), and most of them were organ specific (Figure 5G). Salicylate was one among 13 aspirin metabolites that were clearly detectable in all investigated organs (Figure 5H; Table S2). In line with our *in vitro* observations and with the evidence that, in patients taking up to 3 g aspirin/day, salicylate reaches 1–3 mM concentration in plasma (Shirakawa et al., 2016), a dose range in which
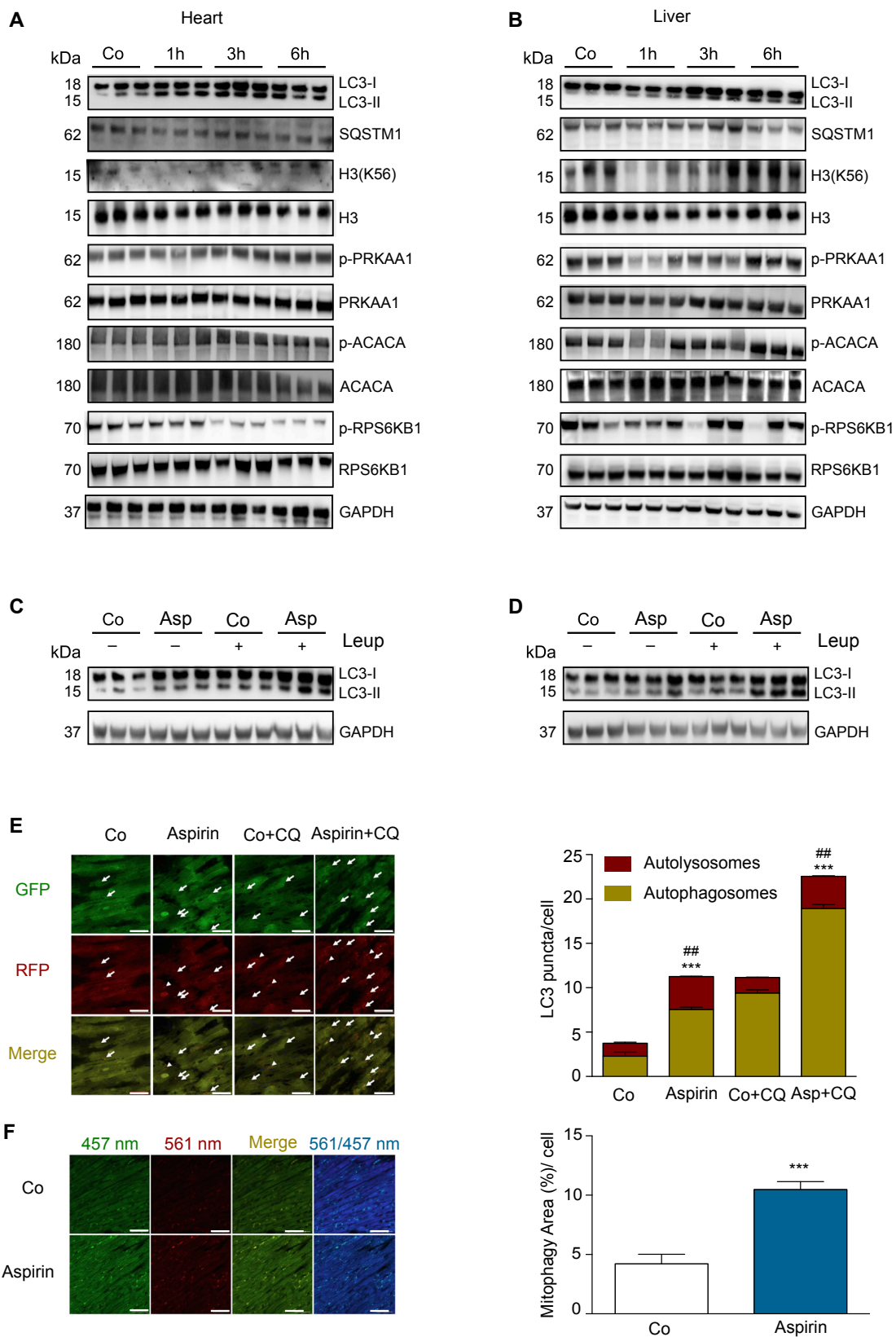

Figure 3. EP300 Inhibition Is Epistatic to Salicylate-Induced Autophagy

(A and B) Administration of increasing doses of salicylate to human HCT116 colorectal cancer cells stably expressing GFP-LC3 induces autophagy in wild-type (WT), yet it fails to further stimulate autophagy in EP300 knockout (KO-EP300) cells. Representative images (A, from Co versus 5-mM salicylate dose in the presence of bafilomycin A1) and quantitation of the number of GFP-LC3 puncta (B) are reported. Results (means ± SD) are from one representative experiment (*p < 0.05, unpaired t test compared with respective control conditions; **p < 0.01, unpaired t test compared with respective control conditions; ***p < 0.001, unpaired t test compared with respective control conditions; ###p < 0.001, unpaired t test compared with WT control cells).

(C and D) Computational docking model of the interactions between the CoA-binding site of EP300 with Lys-CoA (C) or salicylate (D). Two amino acid residues suggested to be important for the interaction with salicylate, but not for that with AcCoA, were mutated (Y1414A and W1466K), as described in the corresponding Experimental Procedures.

(E and F) HCT116 KO-EP300 cells, untagged (E) or stably expressing GFP-LC3 (F), were transfected with a vector carrying wild-type (WT), Y1414A, W1466K, or double-mutated (DM) forms of EP300. In EP300-KO HCT116 cells transfected with the W1466K or EP300 DM forms, salicylate-induced autophagy is partially or completely abrogated, respectively, as measured by following the LC3I-to-LC3II conversion by immunoblotting (E) and the formation of GFP-LC3 positive puncta (in the presence or absence of BafA1) (F). Representative immunoblots (E) and automated videomicroscopy-based quantitation of the number of GFP-LC3 puncta/cell (F) are depicted. Rapamycin (R) was used as a positive control of autophagy induction (means ± SD). One representative experiment is shown (n = 3; *p < 0.05, **p < 0.01, and ***p < 0.001, unpaired t test compared with respective control group).

(G) Salicylate reduces the EP300-dependent acetylation of autophagic protein LC3. HCT116 cells stably expressing GFP-LC3 were incubated for 16 hr with the indicated concentration of salicylate followed by GFP-Trap-based immunoprecipitation. NF medium was used as a negative control of LC3 acetylation. Acetylation status of GFP-LC3 immunoprecipitate was assessed by means of an antibody recognizing acetylated residues on proteins (left panel) and quantified (right panel). Values represent means ± SEM from three independent experiments (normalized on immunoprecipitated GFP levels) (***p < 0.001 and **p < 0.01, one-way ANOVA).

A Heart

B Liver

C

D

E

F

(legend on next page)

this molecule exhibits EP300 inhibitory and pro-autophagic properties, salicylate thus likely represents one of the principal metabolites responsible for aspirin activity. At this stage, it is not clear why some organs are refractory to aspirin-mediated induction of autophagy.

Aspirin Induces Autophagy in *C. elegans* via EP300 Inhibition

Upon treatment with aspirin, autophagic puncta (visualized as a fusion protein between the LC3 worm ortholog LGG-1 and GFP) were significantly upregulated in nematode embryos (Figure 6A). The aspirin-induced increase in LGG-1 puncta was accompanied by the degradation of the autophagic substrate SQST-1 (Figure 6B), and this was still observed after the addition of BafA1, as compared to BafA1-only-treated animals (Figure 6C), yet lost upon silencing of the autophagy essential genes *bec-1* and *atg-7* in the intestine of adult animals (Figure 6D). Consistent with data obtained in mammalian cells, RNAi-mediated silencing of *cbp-1* (the *C. elegans* ortholog of EP300) was sufficient to stimulate autophagy (Figure 6E). Importantly, autophagy mediated by *cbp-1* silencing could not be further enhanced by aspirin treatment, indicating that *cbp-1* inhibition was epistatic to aspirin-induced autophagy (Figure 6E). Salicylate was able to trigger autophagy in nematodes to an extent comparable with aspirin treatment (Figure 6F). In agreement with the notion that aspirin specifically promotes mitophagy in cardiomyocytes, we found that silencing of *dct-1*, a putative ortholog of the mammalian NIX/BNIP3L and BNIP3 and a key mediator of longevity and mitophagy in *C. elegans* (Palikaras et al., 2015), abolished aspirin-induced autophagy (Figure 6G), suggesting that aspirin engages in selective autophagic degradation of mitochondria in nematodes. In support of this observation, we demonstrated that aspirin treatment induced the selective autophagic degradation of the mitochondrial targeted Rosella (mt-Rosella) biosensor (Figure 6H).

DISCUSSION

Based on the results described in this paper, aspirin may be classified as a CRM. Indeed, aspirin fulfills all the criteria of a CRM (Madeo et al., 2014) as it (1) reduces protein acetylation by virtue of its ability to inhibit the acetyltransferase activity of EP300, (2) stimulates autophagic flux, and (3) has no cytotoxic activity.

Caloric restriction-based strategies or periodic fasting have a favorable impact on health and longevity, both in non-human primates (Colman et al., 2009; Mattison et al., 2017) and in human studies (Longo and Mattson, 2014), although studies carried out in different research centers yielded controversial results regarding CR-mediated improved survival outcomes in rhesus monkeys (Mattison et al., 2012). CRMs have been efficiently used to sensitize tumor cells to chemotherapy (Pietrocola et al., 2016), to treat obesity and metabolic syndrome (Cantó et al., 2012), and to prolong health span and lifespan (Eisenberg et al., 2016, 2017; Madeo et al., 2014). Aspirin is known to reduce the occurrence and progression of several human cancer types (Li et al., 2015; Rothwell et al., 2012), to reverse high-fat diet-induced insulin resistance (Kim et al., 2001), and to prolong lifespan in mice (Strong et al., 2008). At this point, it remains to be determined to which extent EP300 inhibition and autophagy activation may effectively contribute to these aspirin effects that apparently transcend its well-established anti-inflammatory effects. Pre-clinical evidence suggests that a brain-permeable aspirin derivative can reduce tau-mediated neurodegeneration in an EP300-dependent fashion (Min et al., 2015). However, the role of autophagy has not been explored in this setting. Epidemiological and experimental data indicate that a high nutritional uptake of the EP300 inhibitor spermidine counteracts cardiac aging, both in humans and rodents (Eisenberg et al., 2016, 2017). In addition, spermidine reduces arteriosclerosis (Michiels et al., 2016) and colon carcinogenesis (Miao et al., 2016) in mouse models. These spermidine effects hence show a notable overlap with those of aspirin, in accord with the observation that both compounds inhibit EP300.

EP300 is a protein that undergoes cytoplasmic-nuclear shuttling and that presumably has rather distinct functions in the cytoplasm and in the nucleus. Indeed, in this latter compartment, EP300 acts as co-factor of several major transcription factors, including tumor protein p53 (TP53), cAMP response element-binding protein (CREB), promyelocytic leukemia (PML), and hypoxia-inducible factor 1 alpha subunit (HIF-1α)

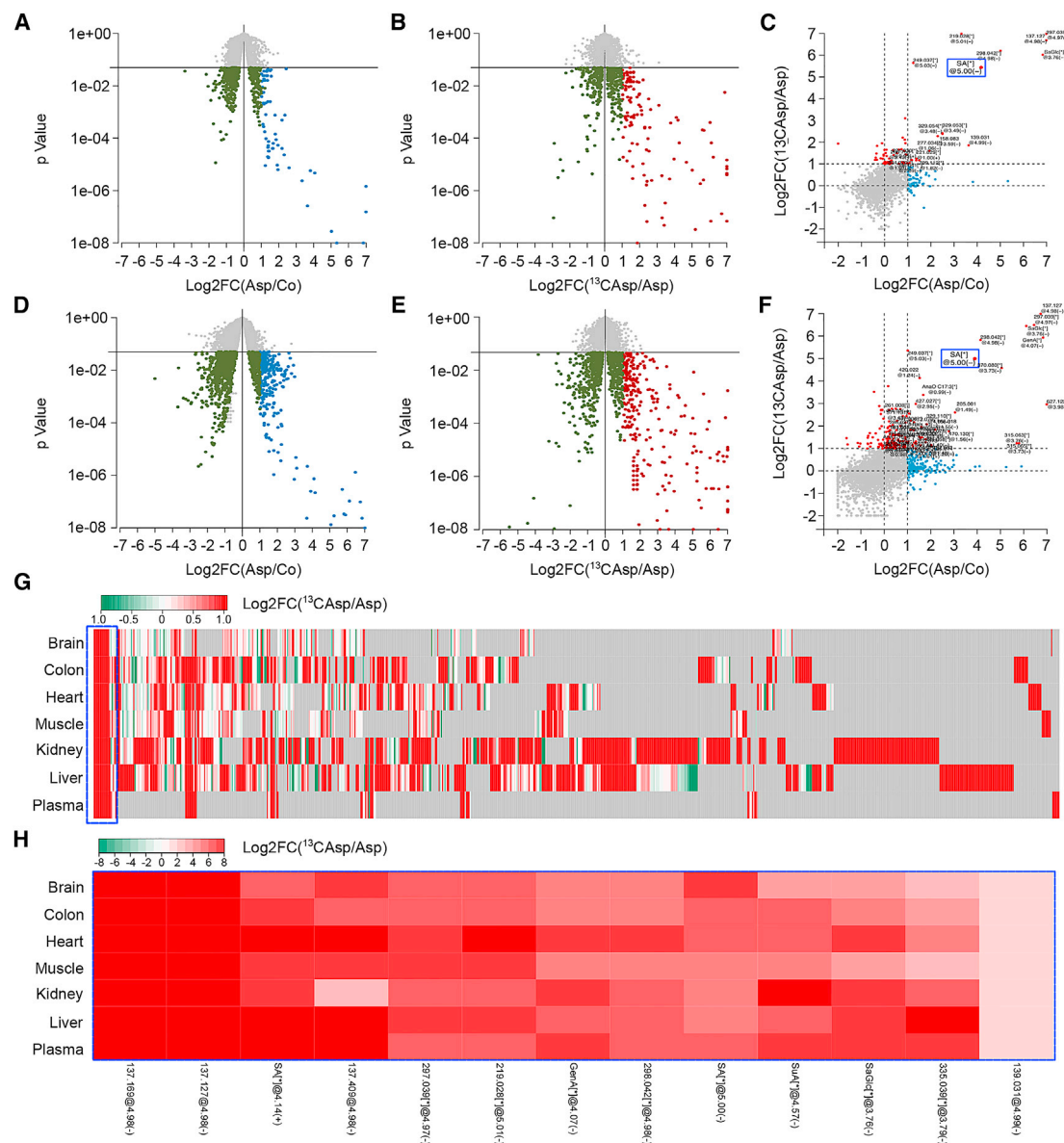**Figure 4. Induction of Autophagy by Acetylsalicylic Acid *In Vivo***

(A and B) Representative immunoblots (n = 3 mice per condition, n = 3 experiments) showing LC3I-to-LC3II conversion and depletion of the autophagic substrate SQSTM1/p62 in the heart (A) and in the liver (B) (1, 3, and 6 hr after intraperitoneal (i.p.) injection of 100 mg/kg aspirin). Autophagy induction *in vivo* is paralleled by a transient decrease in H3K56 acetylation, precedes PRKAA activation (as monitored by upstream kinase-dependent phosphorylation on Thr172 and an increase in PRKAA-mediated ACACA phosphorylation on Ser79), and it is accompanied by a reduction in the mTORC1 substrate PRS6K1. GAPDH levels were monitored to ensure equal protein content. Quantification of (A) and (B) are shown in Figures S3A–S3F and S4A–S4F, respectively.

(C and D) Representative immunoblots (n = 2 experiments, n = 3 mice per group) showing LC3I-to-LC3II conversion in the presence or absence of the protease inhibitor leupeptin (Leup) in the heart (C) and liver (D) 6 hr after aspirin treatment. Quantifications are presented in Figures S3G and S4G, respectively.

(E and F) Long-term aspirin treatment enhances autophagic flux in the heart and stimulates mitophagy.

(E) Transgenic mice expressing the tandem-fluorescent mRFP-GFP-LC3 (Tg-tf-LC3) were treated for 2 weeks with 25 mg/kg aspirin by oral gavage, and autophagic flux was assessed by the injection of chloroquine (10 mg/kg) 4 hr prior to euthanasia. Representative images of fluorescent GFP-LC3 puncta and mRFP-puncta are shown in the left panel. Arrows, autophagosomes; arrowheads, autolysosomes. Values in the right panel represent mean number of autophagosomes (yellow bars) and autolysosomes (red bars) per cell ± SD from one representative experiment (***p < 0.001 and ##p < 0.01, one-way ANOVA compared to respective control conditions.

(F) Evaluation of mitochondrial autophagy by transgenic Mito-Keima mice. 2-month-old C57BL/6J mouse hearts were examined in the control versus aspirin-treated group (n = 3 mice/group). Representative images of Mito-Keima green (457 nm), Mito-Keima red (561 nm), the merged image, and a ratiometric image of red-to-green Mito-Keima (561/457 nm) indicating mitophagy are shown (left panel) and quantified (right panel). Values represent means ± SD from one representative experiment (***p < 0.001, unpaired t test compared to control group). Scale bar, 50 μm.

Figure 5. Metabolomics Analysis of Aspirin-Derived Metabolites

The 6-week old C57BL/6 mice were injected with unlabeled aspirin (Asp) or [^{13}C]-labeled aspirin (^{13}CAsp) (100 mg/kg, i.p.), followed by mass spectrometry.

(A and D) Volcano plots relative to metabolites detected in the heart (A) and in the liver (D) after unlabeled aspirin injection. Log2FC of Asp/Co-downregulated (green) or -upregulated (blue) metabolites with p value < 0.05 is represented.
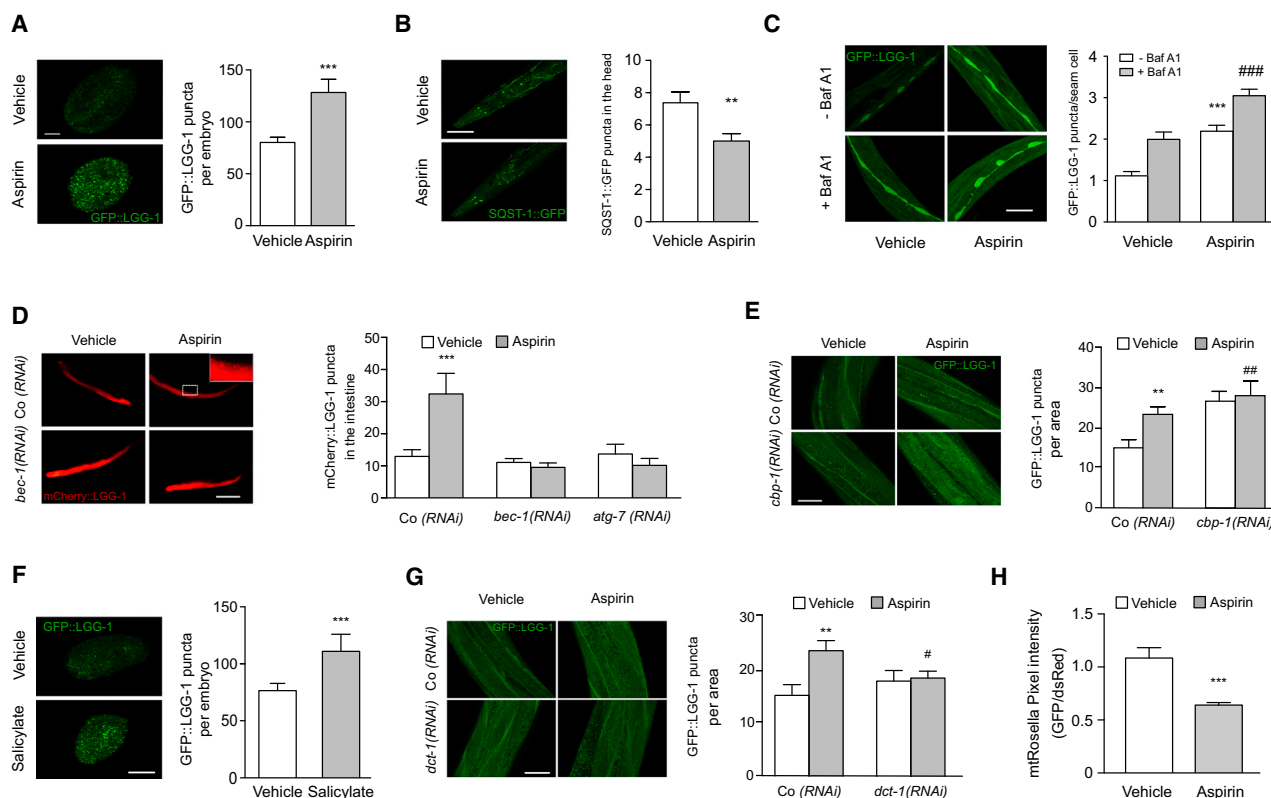
(B and E) Volcano plots relative to metabolites detected in the heart (B) and in the liver (E) after [^{13}C]-labeled aspirin injection. Log2FC of ^{13}CAsp/Asp-downregulated (green) or -upregulated (red) metabolites with p value < 0.05 is depicted.

(C and F) Comparison between ^{13}CAsp/Asp (red) and Asp/Co (blue). Log2FC significantly changed (p value < 0.05) in the heart (C) and in the liver (F) is graphed. The blue box highlights salicylate, which represents a commonly upregulated metabolite in all organs assessed.

(G and H) Heatmap (Log2FC) of ^{13}CAsp/Asp metabolites in different organs (G) is shown. [^{13}C]-Aspirin administration allows the identification of bona fide aspirin-derived metabolites, which are distributed in an organ-specific fashion. Common upregulated metabolites are highlighted with a blue box. Magnification is shown in (H). Pre-annotated metabolites are as follows: SA[*]@4.14, salicylic acid, positive mode; GenA[*]@4.07(-), gentisic/2-pyrocatechuic acid; SA[*]@5.00(-), salicylic acid, negative mode; SuA[*]@4.57(-), salicyluric acid; and SaGlc[*]@3.76(-), salicylate glucuronide. Details are available in Table S2.

(Chan and La Thangue, 2001). While the immediate autophagy-inducing function of EP300 can be explained by its cytoplasmic action (given that enucleated cells still manifest autophagy induction upon EP300 inhibition) (Mariño et al.,

2014), it is well possible that the long-term effects of aspirin also involve transcriptional reprogramming (Voora et al., 2016) that is influenced by EP300. Future work will have to address these possibilities.

Figure 6. Aspirin Activates Autophagy in *C. elegans* and Reduces Aging in an Autophagy Gene-Dependent Manner

(A) Representative confocal images (left panel) of GFP::LGG-1-expressing embryos treated with 1 mM aspirin compared to vehicle and quantification of GFP::LGG-1 puncta per embryo (right panel). Scale bar, 10 μm. Data represent means ± SEM of at least 15 images obtained across 2 independent experiments (***p < 0.001, unpaired t test compared to vehicle-treated nematodes).

(B) Aspirin administration promotes proficient autophagic flux, as monitored by the reduction in levels of SQST-1/p62 autophagic substrate in the pharyngeal region of SQST-1::GFP transgenic animals at day 1 of adulthood. Representative images (left panel) and quantification (right panel) are shown. Scale bar, 20 μm. Data represent means ± SEM of n = 52 worms per group, pooled from three independent experiments (**p < 0.01, unpaired t test).

(C) Aspirin stimulates autophagic flux. Representative confocal images (left panel) and quantification (right panel) of GFP::LGG-1 puncta in the hypodermal seam cells of L3–L4 larvae treated or not from the L4 stage of the first generation with 1 mM aspirin in the absence or in the presence of bafilomycin A1 (100 μg/mL). Scale bar, 10 μm. Data represent means ± SEM of n = 196–329 seam cells, pooled from two independent experiments (***p < 0.001, one-way ANOVA compared to vehicle – BafA1 treatment; ###p < 0.001, one-way ANOVA compared to vehicle + BafA1 treatment).

(D) Administration of aspirin induces the autophagy-dependent increase of p$_{nhx-2}$mCherry::LGG-1 puncta in the intestine of 2-day-old adults, which is lost upon siRNA-mediated depletion of BEC-1 and ATG-7. Epifluorescence images are depicted in the left panel (magnification indicates mCherry::LGG-1 puncta as detected in aspirin-treated worms) and quantified in the right panel. Scale bar, 100 μm. Data represent means ± SEM of n = 15–28 worms per group, pooled from two independent experiments (***p < 0.001, one-way ANOVA compared to vehicle Co *RNAi*).

(E) CBP-1 depletion is epistatic to aspirin-induced autophagy. RNAi-driven elimination of *cbp-1* in transgenic animals expressing the GFP::LGG-1 reporter leads to an increase in the number of GFP::LGG-1 puncta, which are not further increased by aspirin administration. Representative confocal images (left panel) and corresponding quantification (right panel) are shown. Scale bar, 10 μm. Data represent means ± SEM (##p < 0.005 and **p < 0.01, unpaired t test compared to Co *RNAi*-vehicle condition).

(F) Salicylate induces autophagy in *C. elegans*. Representative confocal images (left panel) and corresponding quantification (right panel) of GFP::LGG-1 puncta in transgenic embryos treated with vehicle or salicylate (1 mM). Vehicle bar is shared with experiments depicted in (A) as assays were conducted in parallel. Data represent means ± SEM of at least 15 images obtained in 2 independent experiments (***p < 0.001, unpaired t test compared to vehicle-treated nematodes).

(G) Knockdown of *dct-1*, a putative ortholog to the mammalian NIX/BNIP3L and BNIP3, reduces the number of GFP::LGG-1-positive foci in the epidermis of aspirin-treated young adult wild-type animals. Representative confocal images (left panel) and corresponding quantification (right panel) are depicted. Scale bar, 10 μm. Values represent means ± SEM (**p < 0.01, unpaired t test compared with Co *RNAi* vehicle; #p < 0.05, unpaired t test compared with Co *RNAi* aspirin). Co *RNAi* vehicle and aspirin bars are shared with data depicted in (E), as assays were conducted in parallel.

(H) Mitophagy is induced in nematodes treated with aspirin. Transgenic animals expressing the mt-Rosella biosensor in the body wall muscle cells were treated with 1 mM aspirin or vehicle control. Mitophagy induction is signified by the reduction of the ratio between pH-sensitive GFP to pH-insensitive DsRed. Data represent means ± SEM of n = 22–33 worms per group, pooled from two independent experiments (***p < 0.001, unpaired t test).

Untargeted metabolomics analysis revealed that aspirin-derived metabolites are generated in a highly organ-specific fashion, although some metabolites, including salicylate, were found ubiquitously. Future studies are required to identify the molecular structure of all aspirin metabolites and to measure their pharmacological effects. In particular, it will be interesting to learn which aspirin metabolites have autophagy-stimulating properties.

EXPERIMENTAL PROCEDURES

Mouse Strains and Housing

Mice were maintained in specific pathogen-free conditions in a temperature-controlled environment with 12-hr light/dark cycles, and they received food and water *ad libitum* (except as noted). Animal experiments were in compliance with the EU Directive 63/2010 and protocols were approved (APAFIS 2314-2015101617187579v1) by the Ethical Committee of the Cordeliers Research Center (CEEA Darwin 5, registered at the French Ministry of Research). The 6- to 7-week-old male WT C57BL/6 mice were obtained from Envigo France (Gannat, France). For cardiac mitophagy assessment, transgenic mice with cardiac-specific expression of Mito-Keima were generated on a C57BL/6J background with the murine α-myosin heavy-chain promoter (experiments were approved by the Rutgers-New Jersey Medical School's Institutional Animal Care and Use Committee). For the evaluation of the autophagic flux, transgenic mice with cardiac-specific expression of tf-LC3 (Tg-tf-LC3) were generated on an FVB background with the murine α-myosin heavy-chain promoter, kindly provided by Dr. L. Robbins (Children's Hospital, Cincinnati, OH) (experiments were approved by the Rutgers-New Jersey Medical School's Institutional Animal Care and Use Committee).

In Vitro Acetylation Assay

Recombinant GST-EP300 fusion protein, corresponding to the amino acids 1,066–1,707 (14-418, Millipore), was assessed for its acetyltransferase activity on the EP300 natural substrates recombinant histone H3 protein (M2503S, New England Biolabs). Briefly, 1 μg EP300 Histone acetyl transferase (HAT) domain was incubated in the presence of an HAT assay buffer (250 mM Tris-HCl [pH 8.0], 50% glycerol, 0.5 mM EDTA, and 5 mM dithiothreitol), 1 μg substrate protein, and two different concentrations of AcCoA (A2056, Sigma-Aldrich) for 1 hr at 30°C in the presence of AA, C646, and sodium salicylate. The reaction was stopped by adding 4× SDS buffer and boiling the samples. Acetylation of substrate proteins was measured by immunoblotting using specific antibodies against H3K56.

AHA-Protein Labeling

L-azidohomoalanine (L-AHA) (C10102, Thermo Fisher Scientific) labeling to measure autophagic protein degradation was performed as described in Wang et al. (2017), except with an extension of chase time to 18 hr in adaptation to U2OS cells. After chase, U2OS cells were treated for 16 hr in the presence of 5 mM sodium salicylate or nutrient-free medium. Chemoselective ligation between an AHA azido moiety and a fluorescently tagged alkyne probe was used to monitor fluoresence intensity per cell using an automated microscope Image Xpress Micro XLS (Molecular Devices).

Quantification and Statistical Analysis

Unless otherwise specified, quantitative data are presented as mean ± SD and significance was assessed by unpaired t test by means of Prism software. Additional details are available in the corresponding figure legends and in the Supplemental Experimental Procedures.

SUPPLEMENTAL INFORMATION

Supplemental Information includes Supplemental Experimental Procedures, six figures, and two tables and can be found with this article online at https://doi.org/10.1016/j.celrep.2018.02.024.

ACKNOWLEDGMENTS

AUTHOR CONTRIBUTIONS

F.P., F.C., M.M., S.L., G.C., N.D., F.L., S.A.M., and G.M. performed the experiments. In particular, F.P. performed immunoblots, siRNA transfections, and automated video microscopy; F.C. conducted immunoblots; M.M. performed all *C. elegans* experiments; M.T. conducted mtKeima and tgGFP-RFP transgenic mouse experiments; G.C. performed the ethyl-salicylate-related experiment; F.L. conducted AHA-labeling; N.D. performed [14]-C-valine long-lived protein degradation assays; S.L. conducted in vitro cell-free assays and EP300 mutant experiments; S.A.M. performed in vivo experiments and immunoblots; and D.P.E., S.D., and N.B. conducted metabolomic analyses and statistics. N.A. and R.K. designed the docking modeling for the rational design of EP300 mutants. G.M., F.M., M.C.M., P.C., and J.S. helped to design the study. F.P., M.M., N.T., and G.K. conceived the study, analyzed the data, and wrote the paper.

DECLARATION OF INTERESTS

G.K. has received research support from and consults for Bayer. The other authors declare no competing interests.

REFERENCES

Ali, B., and Kaur, S. (1983). Mammalian tissue acetylsalicylic acid esterase(s): identification, distribution and discrimination from other esterases. J. Pharmacol. Exp. Ther. *226*, 589–594.

Baron, J.A., Cole, B.F., Sandler, R.S., Haile, R.W., Ahnen, D., Bresalier, R., McKeown-Eyssen, G., Summers, R.W., Rothstein, R., Burke, C.A., et al. (2003). A randomized trial of aspirin to prevent colorectal adenomas. N. Engl. J. Med. *348*, 891–899.

Bauvy, C., Meijer, A.J., and Codogno, P. (2009). Assaying of autophagic protein degradation. Methods Enzymol. *452*, 47–61.

Bowers, E.M., Yan, G., Mukherjee, C., Orry, A., Wang, L., Holbert, M.A., Crump, N.T., Hazzalin, C.A., Liszczak, G., Yuan, H., et al. (2010). Virtual ligand screening of the p300/CBP histone acetyltransferase: identification of a selective small molecule inhibitor. Chem. Biol. *17*, 471–482.

Cantó, C., Houtkooper, R.H., Pirinen, E., Youn, D.Y., Oosterveer, M.H., Cen, Y., Fernandez-Marcos, P.J., Yamamoto, H., Andreux, P.A., Cettour-Rose, P., et al. (2012). The NAD(+) precursor nicotinamide riboside enhances oxidative metabolism and protects against high-fat diet-induced obesity. Cell Metab. *15*, 838–847.

Cerletti, C., Bonati, M., del Maschio, A., Galletti, F., Dejana, E., Tognoni, G., and de Gaetano, G. (1984). Plasma levels of salicylate and aspirin in healthy volunteers: relevance to drug interaction on platelet function. J. Lab. Clin. Med. *103*, 869–877.

Chan, H.M., and La Thangue, N.B. (2001). p300/CBP proteins: HATs for transcriptional bridges and scaffolds. J. Cell Sci. *114*, 2363–2373.

Colman, R.J., Anderson, R.M., Johnson, S.C., Kastman, E.K., Kosmatka, K.J., Beasley, T.M., Allison, D.B., Cruzen, C., Simmons, H.A., Kemnitz, J.W., and Weindruch, R. (2009). Caloric restriction delays disease onset and mortality in rhesus monkeys. Science *325*, 201–204.

Din, F.V., Valanciute, A., Houde, V.P., Zibrova, D., Green, K.A., Sakamoto, K., Alessi, D.R., and Dunlop, M.G. (2012). Aspirin inhibits mTOR signaling, activates AMP-activated protein kinase, and induces autophagy in colorectal cancer cells. Gastroenterology *142*, 1504–1515.e3.

Dupont, N., Leroy, C., Hamaï, A., and Codogno, P. (2017). Long-Lived Protein Degradation During Autophagy. Methods Enzymol. *588*, 31–40.

Egan, D.F., Shackelford, D.B., Mihaylova, M.M., Gelino, S., Kohnz, R.A., Mair, W., Vasquez, D.S., Joshi, A., Gwinn, D.M., Taylor, R., et al. (2011). Phosphorylation of ULK1 (hATG1) by AMP-activated protein kinase connects energy sensing to mitophagy. Science *331*, 456–461.

Eisenberg, T., Knauer, H., Schauer, A., Büttner, S., Ruckenstuhl, C., Carmona-Gutierrez, D., Ring, J., Schroeder, S., Magnes, C., Antonacci, L., et al. (2009). Induction of autophagy by spermidine promotes longevity. Nat. Cell Biol. *11*, 1305–1314.

Eisenberg, T., Schroeder, S., Andryushkova, A., Pendl, T., Küttner, V., Bhukel, A., Mariño, G., Pietrocola, F., Harger, A., Zimmermann, A., et al. (2014). Nucleocytosolic depletion of the energy metabolite acetyl-coenzyme a stimulates autophagy and prolongs lifespan. Cell Metab. *19*, 431–444.

Eisenberg, T., Abdellatif, M., Schroeder, S., Primessnig, U., Stekovic, S., Pendl, T., Harger, A., Schipke, J., Zimmermann, A., Schmidt, A., et al. (2016). Cardioprotection and lifespan extension by the natural polyamine spermidine. Nat. Med. *22*, 1428–1438.

Eisenberg, T., Abdellatif, M., Zimmermann, A., Schroeder, S., Pendl, T., Harger, A., Stekovic, S., Schipke, J., Magnes, C., Schmidt, A., et al. (2017). Dietary spermidine for lowering high blood pressure. Autophagy *13*, 767–769.

Ganapathy, V., Thangaraju, M., Gopal, E., Martin, P.M., Itagaki, S., Miyauchi, S., and Prasad, P.D. (2008). Sodium-coupled monocarboxylate transporters in normal tissues and in cancer. AAPS J. *10*, 193–199.

Ghizzoni, M., Boltjes, A., Graaf, Cd., Haisma, H.J., and Dekker, F.J. (2010). Improved inhibition of the histone acetyltransferase PCAF by an anacardic acid derivative. Bioorg. Med. Chem. *18*, 5826–5834.

Hariharan, N., Zhai, P., and Sadoshima, J. (2011). Oxidative stress stimulates autophagic flux during ischemia/reperfusion. Antioxid. Redox Signal. *14*, 2179–2190.

Hawley, S.A., Fullerton, M.D., Ross, F.A., Schertzer, J.D., Chevtzoff, C., Walker, K.J., Peggie, M.W., Zibrova, D., Green, K.A., Mustard, K.J., et al. (2012). The ancient drug salicylate directly activates AMP-activated protein kinase. Science *336*, 918–922.

He, C., and Klionsky, D.J. (2009). Regulation mechanisms and signaling pathways of autophagy. Annu. Rev. Genet. *43*, 67–93.

He, C., Bassik, M.C., Moresi, V., Sun, K., Wei, Y., Zou, Z., An, Z., Loh, J., Fisher, J., Sun, Q., et al. (2012). Exercise-induced BCL2-regulated autophagy is required for muscle glucose homeostasis. Nature *481*, 511–515.

Heilbronn, L.K., and Ravussin, E. (2003). Calorie restriction and aging: review of the literature and implications for studies in humans. Am. J. Clin. Nutr. *78*, 361–369.

Heintz, C., Doktor, T.K., Lanjuin, A., Escoubas, C., Zhang, Y., Weir, H.J., Dutta, S., Silva-García, C.G., Bruun, G.H., Morantte, I., et al. (2017). Splicing factor 1 modulates dietary restriction and TORC1 pathway longevity in C. elegans. Nature *541*, 102–106.

Higgs, G.A., Salmon, J.A., Henderson, B., and Vane, J.R. (1987). Pharmacokinetics of aspirin and salicylate in relation to inhibition of arachidonate cyclooxygenase and antiinflammatory activity. Proc. Natl. Acad. Sci. USA *84*, 1417–1420.

Huang, R., Xu, Y., Wan, W., Shou, X., Qian, J., You, Z., Liu, B., Chang, C., Zhou, T., Lippincott-Schwartz, J., and Liu, W. (2015). Deacetylation of nuclear LC3 drives autophagy initiation under starvation. Mol. Cell *57*, 456–466.

Katayama, H., Kogure, T., Mizushima, N., Yoshimori, T., and Miyawaki, A. (2011). A sensitive and quantitative technique for detecting autophagic events based on lysosomal delivery. Chem. Biol. *18*, 1042–1052.

Kim, J., and Guan, K.L. (2013). AMPK connects energy stress to PIK3C3/VPS34 regulation. Autophagy *9*, 1110–1111.

Kim, J.K., Kim, Y.J., Fillmore, J.J., Chen, Y., Moore, I., Lee, J., Yuan, M., Li, Z.W., Karin, M., Perret, P., et al. (2001). Prevention of fat-induced insulin resistance by salicylate. J. Clin. Invest. *108*, 437–446.

Kim, J., Kundu, M., Viollet, B., and Guan, K.L. (2011). AMPK and mTOR regulate autophagy through direct phosphorylation of Ulk1. Nat. Cell Biol. *13*, 132–141.

Klionsky, D.J., Abdelmohsen, K., Abe, A., Abedin, M.J., Abeliovich, H., Acevedo Arozena, A., Adachi, H., Adams, C.M., Adams, P.D., Adeli, K., et al. (2016). Guidelines for the use and interpretation of assays for monitoring autophagy (3rd edition). Autophagy *12*, 1–222.

Kopp, E., and Ghosh, S. (1994). Inhibition of NF-kappa B by sodium salicylate and aspirin. Science *265*, 956–959.

Lamming, D.W., Ye, L., Sabatini, D.M., and Baur, J.A. (2013). Rapalogs and mTOR inhibitors as anti-aging therapeutics. J. Clin. Invest. *123*, 980–989.

Lee, I.H., and Finkel, T. (2009). Regulation of autophagy by the p300 acetyltransferase. J. Biol. Chem. *284*, 6322–6328.

Li, P., Wu, H., Zhang, H., Shi, Y., Xu, J., Ye, Y., Xia, D., Yang, J., Cai, J., and Wu, Y. (2015). Aspirin use after diagnosis but not prediagnosis improves established colorectal cancer survival: a meta-analysis. Gut *64*, 1419–1425.

Longo, V.D., and Mattson, M.P. (2014). Fasting: molecular mechanisms and clinical applications. Cell Metab. *19*, 181–192.

López-Otín, C., Galluzzi, L., Freije, J.M.P., Madeo, F., and Kroemer, G. (2016). Metabolic Control of Longevity. Cell *166*, 802–821.

Madeo, F., Pietrocola, F., Eisenberg, T., and Kroemer, G. (2014). Caloric restriction mimetics: towards a molecular definition. Nat. Rev. Drug Discov. *13*, 727–740.

Mariño, G., Pietrocola, F., Eisenberg, T., Kong, Y., Malik, S.A., Andryushkova, A., Schroeder, S., Pendl, T., Harger, A., Niso-Santano, M., et al. (2014). Regulation of autophagy by cytosolic acetyl-coenzyme A. Mol. Cell *53*, 710–725.

Mattison, J.A., Roth, G.S., Beasley, T.M., Tilmont, E.M., Handy, A.M., Herbert, R.L., Longo, D.L., Allison, D.B., Young, J.E., Bryant, M., et al. (2012). Impact of caloric restriction on health and survival in rhesus monkeys from the NIA study. Nature *489*, 318–321.

Mattison, J.A., Colman, R.J., Beasley, T.M., Allison, D.B., Kemnitz, J.W., Roth, G.S., Ingram, D.K., Weindruch, R., de Cabo, R., and Anderson, R.M. (2017). Caloric restriction improves health and survival of rhesus monkeys. Nat. Commun. *8*, 14063.

Miao, H., Ou, J., Peng, Y., Zhang, X., Chen, Y., Hao, L., Xie, G., Wang, Z., Pang, X., Ruan, Z., et al. (2016). Macrophage ABHD5 promotes colorectal cancer growth by suppressing spermidine production by SRM. Nat. Commun. *7*, 11716.

Michiels, C.F., Kurdi, A., Timmermans, J.P., De Meyer, G.R.Y., and Martinet, W. (2016). Spermidine reduces lipid accumulation and necrotic core formation in atherosclerotic plaques via induction of autophagy. Atherosclerosis *251*, 319–327.

Min, S.W., Chen, X., Tracy, T.E., Li, Y., Zhou, Y., Wang, C., Shirakawa, K., Minami, S.S., Defensor, E., Mok, S.A., et al. (2015). Critical role of acetylation in tau-mediated neurodegeneration and cognitive deficits. Nat. Med. *21*, 1154–1162.

Mizushima, N., and Komatsu, M. (2011). Autophagy: renovation of cells and tissues. Cell *147*, 728–741.

Morselli, E., Mariño, G., Bennetzen, M.V., Eisenberg, T., Megalou, E., Schroeder, S., Cabrera, S., Bénit, P., Rustin, P., Criollo, A., et al. (2011). Spermidine and resveratrol induce autophagy by distinct pathways converging on the acetylproteome. J. Cell Biol. *192*, 615–629.

Ogawa, H., Nakayama, M., Morimoto, T., Uemura, S., Kanauchi, M., Doi, N., Jinnouchi, H., Sugiyama, S., and Saito, Y.; Japanese Primary Prevention of
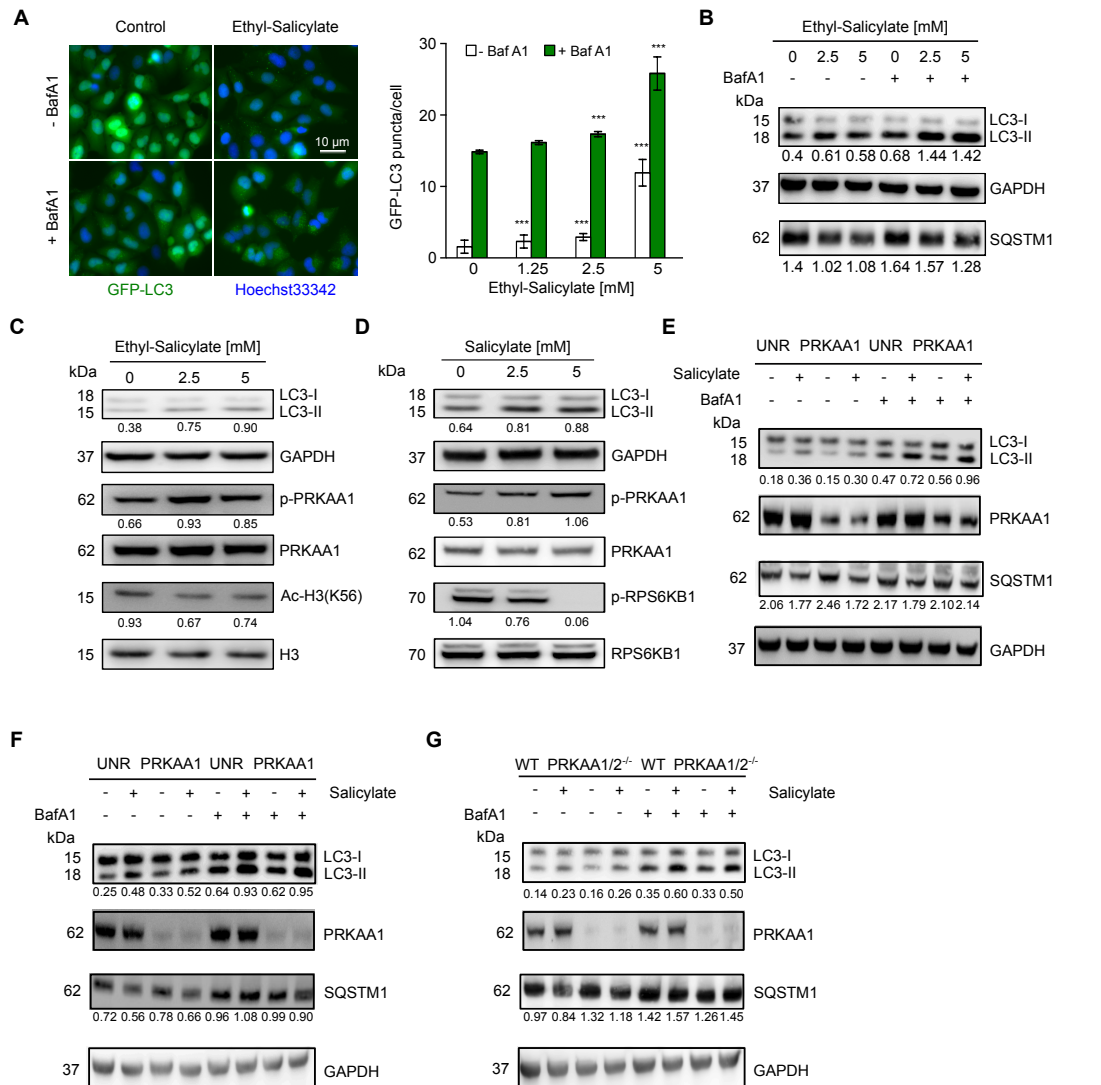
Atherosclerosis With Aspirin for Diabetes (JPAD) Trial Investigators (2008). Low-dose aspirin for primary prevention of atherosclerotic events in patients with type 2 diabetes: a randomized controlled trial. JAMA *300*, 2134–2141.

Palikaras, K., Lionaki, E., and Tavernarakis, N. (2015). Coordination of mitophagy and mitochondrial biogenesis during ageing in C. elegans. Nature *521*, 525–528.

Pan, H., Cai, N., Li, M., Liu, G.H., and Izpisua Belmonte, J.C. (2013). Autophagic control of cell 'stemness'. EMBO Mol. Med. *5*, 327–331.

Pietrocola, F., Galluzzi, L., Bravo-San Pedro, J.M., Madeo, F., and Kroemer, G. (2015a). Acetyl coenzyme A: a central metabolite and second messenger. Cell Metab. *21*, 805–821.

Pietrocola, F., Lachkar, S., Enot, D.P., Niso-Santano, M., Bravo-San Pedro, J.M., Sica, V., Izzo, V., Maiuri, M.C., Madeo, F., Mariño, G., and Kroemer, G. (2015b). Spermidine induces autophagy by inhibiting the acetyltransferase EP300. Cell Death Differ. *22*, 509–516.

Pietrocola, F., Pol, J., Vacchelli, E., Rao, S., Enot, D.P., Baracco, E.E., Levesque, S., Castoldi, F., Jacquelot, N., Yamazaki, T., et al. (2016). Caloric Restriction Mimetics Enhance Anticancer Immunosurveillance. Cancer Cell *30*, 147–160.

Pyo, J.O., Yoo, S.M., Ahn, H.H., Nah, J., Hong, S.H., Kam, T.I., Jung, S., and Jung, Y.K. (2013). Overexpression of Atg5 in mice activates autophagy and extends lifespan. Nat. Commun. *4*, 2300.

Rothwell, P.M., Wilson, M., Price, J.F., Belch, J.F., Meade, T.W., and Mehta, Z. (2012). Effect of daily aspirin on risk of cancer metastasis: a study of incident cancers during randomised controlled trials. Lancet *379*, 1591–1601.

Rubinsztein, D.C., Mariño, G., and Kroemer, G. (2011). Autophagy and aging. Cell *146*, 682–695.

Sandler, R.S., Halabi, S., Baron, J.A., Budinger, S., Paskett, E., Keresztes, R., Petrelli, N., Pipas, J.M., Karp, D.D., Loprinzi, C.L., et al. (2003). A randomized trial of aspirin to prevent colorectal adenomas in patients with previous colorectal cancer. N. Engl. J. Med. *348*, 883–890.

Sebti, S., Prébois, C., Pérez-Gracia, E., Bauvy, C., Desmots, F., Pirot, N., Gongora, C., Bach, A.S., Hubberstey, A.V., Palissot, V., et al. (2014). BAT3 modulates p300-dependent acetylation of p53 and autophagy-related protein 7 (ATG7) during autophagy. Proc. Natl. Acad. Sci. USA *111*, 4115–4120.

Shirakabe, A., Fritzky, L., Saito, T., Zhai, P., Miyamoto, S., Gustafsson, A.B., Kitsis, R.N., and Sadoshima, J. (2016a). Evaluating mitochondrial autophagy in the mouse heart. J. Mol. Cell. Cardiol. *92*, 134–139.

Shirakabe, A., Ikeda, Y., Sciarretta, S., Zablocki, D.K., and Sadoshima, J. (2016b). Aging and Autophagy in the Heart. Circ. Res. *118*, 1563–1576.

Shirakawa, K., Wang, L., Man, N., Maksimoska, J., Sorum, A.W., Lim, H.W., Lee, I.S., Shimazu, T., Newman, J.C., Schröder, S., et al. (2016). Salicylate, diflunisal and their metabolites inhibit CBP/p300 and exhibit anticancer activity. eLife *5*, e11156.

Strong, R., Miller, R.A., Astle, C.M., Floyd, R.A., Flurkey, K., Hensley, K.L., Javors, M.A., Leeuwenburgh, C., Nelson, J.F., Ongini, E., et al. (2008). Nordihydroguaiaretic acid and aspirin increase lifespan of genetically heterogeneous male mice. Aging Cell *7*, 641–650.

Sun, T., Li, X., Zhang, P., Chen, W.D., Zhang, H.L., Li, D.D., Deng, R., Qian, X.J., Jiao, L., Ji, J., et al. (2015). Acetylation of Beclin 1 inhibits autophagosome maturation and promotes tumour growth. Nat. Commun. *6*, 7215.

Sun, N., Youle, R.J., and Finkel, T. (2016). The Mitochondrial Basis of Aging. Mol. Cell *61*, 654–666.

Voora, D., Rao, A.K., Jalagadugula, G.S., Myers, R., Harris, E., Ortel, T.L., and Ginsburg, G.S. (2016). Systems Pharmacogenomics Finds RUNX1 Is an Aspirin-Responsive Transcription Factor Linked to Cardiovascular Disease and Colon Cancer. EBioMedicine *11*, 157–164.

Wang, J., Zhang, J., Lee, Y.M., Ng, S., Shi, Y., Hua, Z.C., Lin, Q., and Shen, H.M. (2017). Nonradioactive quantification of autophagic protein degradation with L-azidohomoalanine labeling. Nat. Protoc. *12*, 279–288.

Wood, J.G., Rogina, B., Lavu, S., Howitz, K., Helfand, S.L., Tatar, M., and Sinclair, D. (2004). Sirtuin activators mimic caloric restriction and delay ageing in metazoans. Nature *430*, 686–689.

Supplemental Information

Aspirin Recapitulates Features
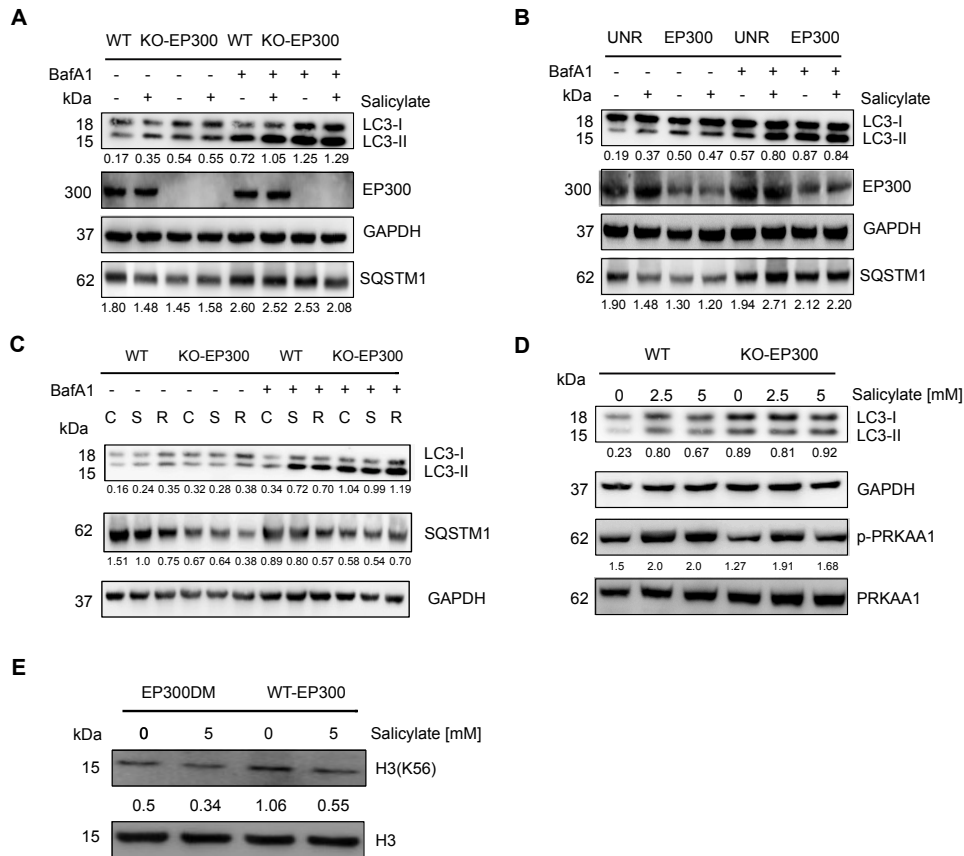
# of Caloric Restriction

Federico Pietrocola, Francesca Castoldi, Maria Markaki, Sylvie Lachkar, Guo Chen, David P. Enot, Sylvere Durand, Noelie Bossut, Mingming Tong, Shoaib A. Malik, Friedemann Loos, Nicolas Dupont, Guillermo Mariño, Nejma Abdelkader, Frank Madeo, Maria Chiara Maiuri, Romano Kroemer, Patrice Codogno, Junichi Sadoshima, Nektarios Tavernarakis, and Guido Kroemer
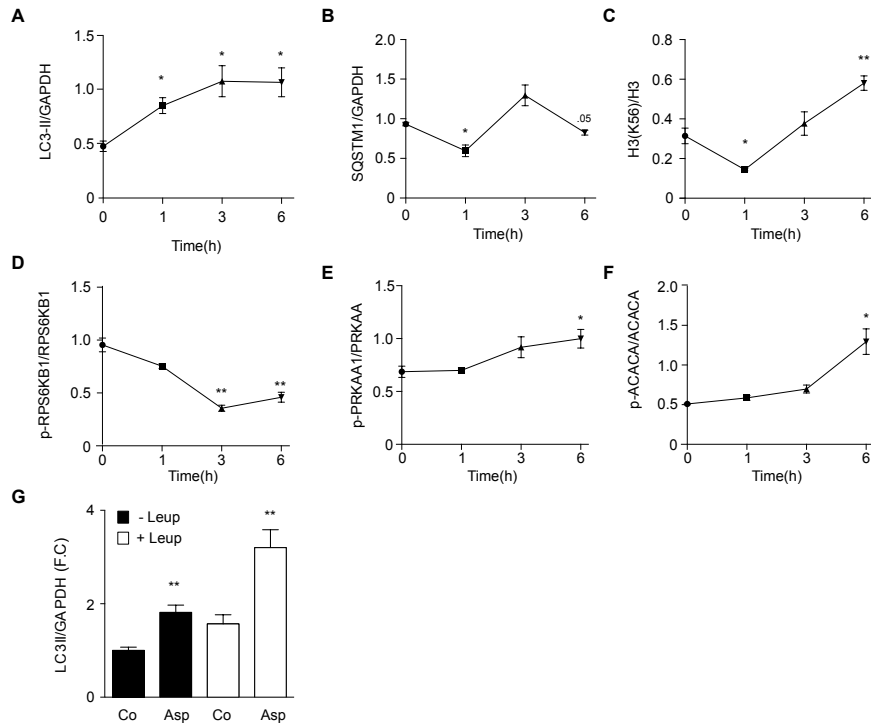
Supplemental Figure 1 (related to Figure 2 and 3). Ethyl-Salicylate induces autophagic flux and inhibits EP300. (**A**) U2OS cells expressing green fluorescent protein (GFP)-LC3 were treated with ethyl-salicylate for 8 h. Addition of Bafilomycin A1 allowed measuring autophagic flux. Representative images (left panel) and quantification (right panel) are shown. Data represent means ± SD from one representative experiment. *** $p < 0.001$; (unpaired t test, as compared with control condition). (**B,C**) HCT116 human colorectal cells were incubated for 8 hours in presence of growing concentrations of ethyl-salicylate. (**B**) Representative immunoblots of three independent experiments showing LC3I to LC3II conversion (in presence or absence of BafA1), (**C**) reduction in the acetylation levels of the EP300 substrate H3K56, (**B**) depletion of the autophagic substrate SQSTM1 and (**C**) activation of PRKAA, as monitored by Thr172 phosphorylation. (**D**) Salicylate modulates nutrient-sensing signaling pathways. Treatment of HCT116 with salicylate promotes the activation of
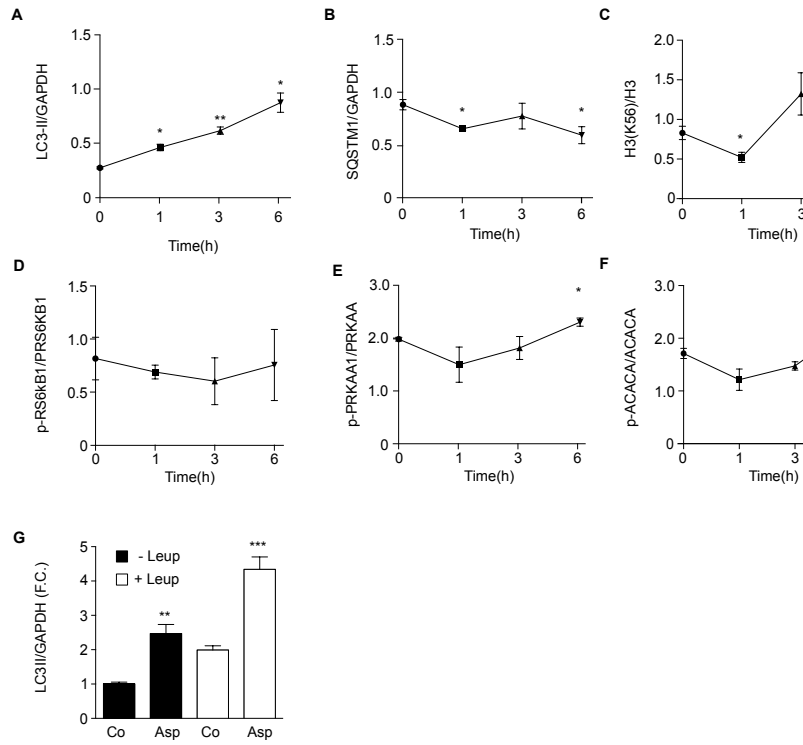
autophagy (as monitored by LC3-I to LC3-II conversion) along with the activation of PRKAA and the inhibition of mTORC1 signaling (as monitored by a decrease in Thr389 phosphorylation of p70 S6 Kinase [PRS6K1]). (**E**) Salicylate-induced autophagy does not require PRKAA activation. HCT116 cells were transfected with an unrelated (UNR) or with a small interfering RNA (siRNA) targeting PRKAA α1 subunit, followed by treatment with of salicylate for 16 hours. Representative immunoblots of three independent experiments showing the increased LC3I to LC3II conversion (in presence or absence of BafA1), the autophagy-dependent degradation of SQSTM1/p62 and the effective silencing of PRKAA1. (**F**) U2OS cells were transfected with an unrelated (UNR) or with a small interfering RNA (siRNA) sequence targeting PRKAA1 subunit and treated with salicylate. Autophagy and effective PRKAA silencing were monitored as previously described. (**G**) Mouse Embryonic Fibroblasts (MEF) Wild Type (WT) or their PRKAA deficient counterparts (PRKAA1/2$^{-/-}$) were treated for 16 hours with 5 mM salicylate and autophagy was monitored by immunoblotting in presence or absence of BafA1 to measure autophagic flux.
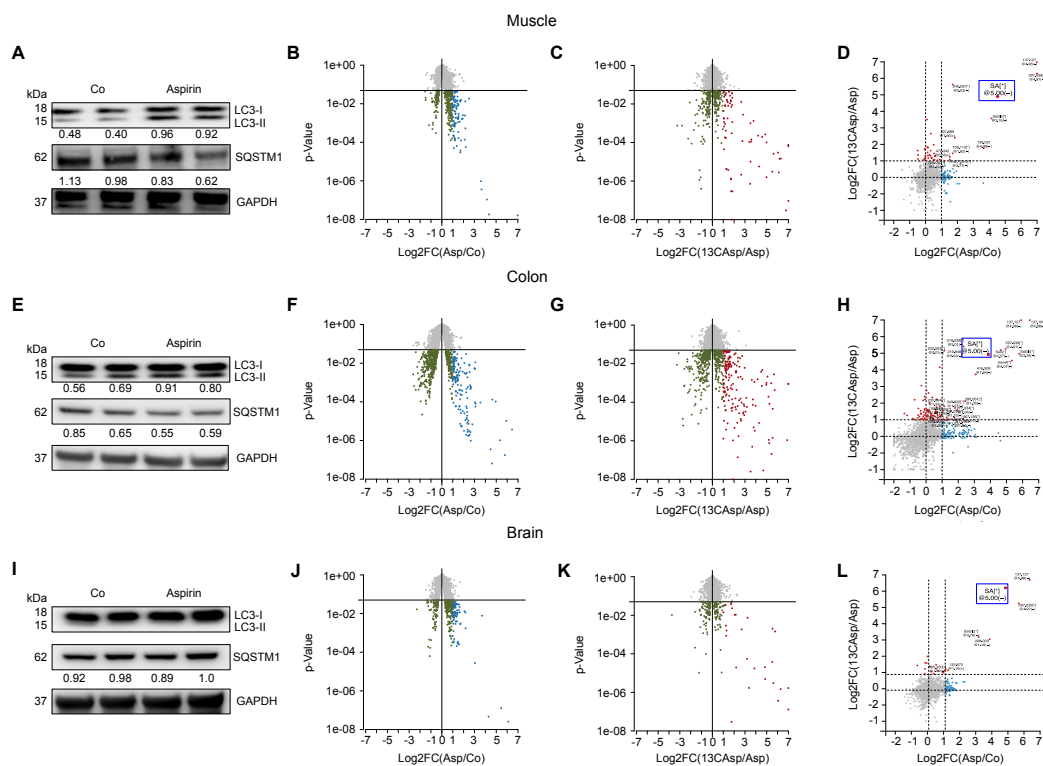
Supplemental Figure 2 (related to Figure 2 and 3) Salicylate-induced autophagy depends on EP300

inhibition (**A**) Administration of salicylate (5 mM) to HCT116 cells induces autophagy in wild type

(WT) yet fails to further up regulate autophagy in KO-EP300 cells, as measured by LC3-I to LC3-II

conversion and SQSTM1 degradation in presence or absence of BafA1 (one representative experiment,

n=3) (**B**) Representative immunoblots of U2OS cells transfected with siRNA sequences specifically

targeting EP300. Salicylate triggers autophagy in unrelated siRNA condition yet does not further

increase autophagy upon EP300 depletion. (**C**) mTORC1 inhibition by Rapamycin induces autophagy

in KO-EP300 cells. EP300 WT cells and their KO-EP300 counterpart were treated with salicylate (S)

and rapamycin (R) and autophagy was monitored in these settings. (n=2) (**D**) Ablation of EP300 does

not affect salicylate-induced activation of PRKAA1. Representative immunoblots (n=2) depicting

LC3I to LC3-II conversion and PRKAA phosphorylation upon treatment with growing doses of

salicylate (**E**) Mutated form of EP300 reduces salicylate binding yet does not impair EP300-

acetyltransferase activity. EP300-KO cells were transfected with WT-EP300 or EP300DM plasmids.

EP300 activity mas monitored through measurement of EP300 substrate H3K56 acetylation.

Supplemental Figure 3 (related to Figure 4). (A-F) Quantification of immunoblots depicted in **Figure 4A**, related to aspirin effect in the heart. Data represent means ± S.E.M. (Standard Error of the Mean) **p< 0.01; *p< 0.05 compared to untreated mice (unpaired *t* test). (**G**) Quantification of immunoblots depicted in **Figure 4C**, related to the measurement of autophagic flux in presence of Leupeptin in the heart. Data represent means ± S.E.M. **p< 0.01 (unpaired *t* test, compared to the respective controls).
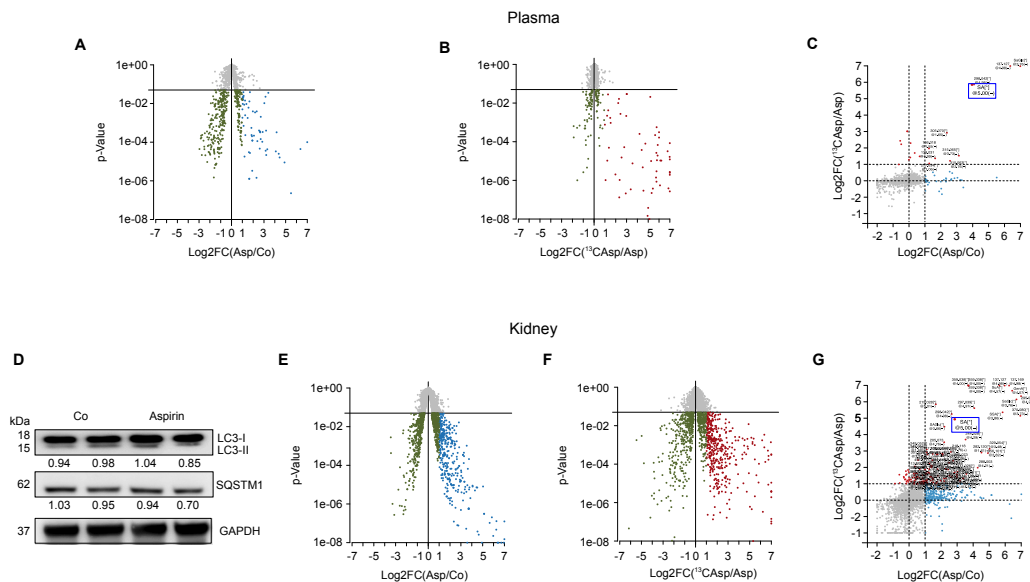
Supplemental Figure 4 (related to Figure 5). Quantification of immunoblots depicted in Figure 4B, related to aspirin effect in the liver. Data represent means means ± S.E.M. **p< 0.01; *p< 0.05 compared to untreated mice (unpaired *t* test). (**G**) Quantification of immunoblots depicted in **Figure 4D**, related to the measurement of autophagic flux in presence of Leupeptin in the liver. Data represent means ± S.E.M. *** p< 0.001; **p< 0.01; (unpaired *t* test, compared to respective controls).

Supplemental Figure 5 (related to Figure 5). Effects of aspirin administration on autophagy and metabolomics analysis of aspirin derived metabolites in muscle, colon and brain. (**A,E,I**). Immunoblots from one representative experiment (n=2) depicting LC3-I to LC3-II conversion and SQSTM1 degradation in the indicated organs one hour after aspirin administration. Aspirin administration triggers autophagy in mice gastrocnemius muscle (**A**) and colon (**E**) yet fails to stimulate autophagy in the brain (**I**). GAPDH was used to monitor equal protein loading among lanes. (**B,F,J**). Volcano plots related to muscle (**B**), colon (**F**) and brain (**J**) of mice injected with unlabeled Aspirin as detected by mass spectrometry coupled with liquid chromatography (LC-MS) are shown. Log2FC of Asp/Co down regulated (green) or up regulated (blue) metabolites < 0.05 is represented. (**C,G,K**) Log2FC of ^{13}CAsp/Asp down regulated (green) or up regulated (red) metabolites with p value < 0.05 in muscle (**C**), colon (**G**) and brain (**K**) as detected by LC-MS after [^{13}C]-Aspirin injection to mice. (**D,H,L**) Log2FC comparison between ^{13}CAsp/Asp (red) and Asp/Co (blue) significantly changed metabolites (p value < 0.05) in muscle (**D**), colon (**H**) and brain (**L**) is depicted. Blue boxes highlight salicylate, which represents a commonly upregulated metabolite in all the organs assessed.

Supplemental Figure 6 (related to Figure 6). Effects of aspirin administration on autophagy and metabolomics analysis of aspirin derived metabolites in mice plasma and kidney. (**A,E**) Volcano plots related to plasma (**A**) and kidney (**E**) of mice injected with unlabeled Aspirin as detected by LC-MS are shown. Log2FC of Asp/Co down regulated (green) or up regulated (blue) with p value < 0.05 is represented. (**B,F**) Log2FC of [13]CAsp/Asp down regulated (green) or up regulated (red) metabolites with p value < 0.05 in plasma (**B**) and kidney (**F**) as detected by LC-MS after [^{13}C]-Aspirin injection to mice. (**C,G**) Log2FC comparison between [13]CAsp/Asp (red) and Asp/Co (blue) (blue) significantly changed metabolites (p value < 0.05) in plasma (**C**) and kidney (**G**) is depicted. Blue boxes highlight salicylate, which represents a commonly upregulated metabolite in all the organs assessed. (**D**) Immunoblots from one representative experiment (n=2) showing LC3-I to LC3-II conversion and SQSTM1 degradation in the kidney of mice one hour after aspirin injection.

Experimental Procedures

Docking computational modeling. In order to test the working hypothesis that Aspirin (and its metabolite salicylate) prevents the binding of Acetyl Coenzyme A to the active site of CBP/EP300, docking of salicylate to EP300 (Protein Database Structure: 3BIY) was analysed by means of Glide extra-precision (Glide XP) software based on the previously described interaction between Lys-CoA and EP300/CBP. (Liu et al., 2008) Docking predicts that the salicylate molecule engages in several interactions with the enzyme, among those some key hydrophobic as well as key polar interactions. Of particular interest are the hydrophobic interactions between Tyr1414 (end-on pi-stacking between CG1-H of Tyr1414 and the pi-cloud of the aromatic ring of salicylate) and salicylate, as well as

between Trp1466 (end-on pi-stacking between C3-H [adjacent to carboxylic acid function] and the pi-cloud of the aromatic 5-ring of Trp1466). In the complex crystal structure of p300/CBP and Lys-CoA (Protein Database Code: 3BIY) Tyr1414 is not involved in particular interactions with the bi-substrate inhibitor, and Trp1466 engages (through its side-chain NH) in a hydrogen bond with the inhibitor. Taking into account the differences in interactions made by Tyr1414 and Trp1466, the following mutations are proposed:

1) Mutation of Tyr1414 into Ala. This mutation should abolish the possibility of hydrophobic or pi-stacking interactions with the salicylate, without having a negative impact on Acetyl-CoA binding

2) Mutation of Trp1466 into Lys. This mutation should abolish the possibility of pi-stacking interactions with the salicylate, while maintaining a polar (hydrogen bonding) interaction with the phosphate of Lys-CoA.

Metabolomics experiment

Sample preparation Tissue

6-weeks old C57BL/6 mice were injected with unlabeled Aspirin or with Acetylsalicylic-α-[^{13}C] on 99 atom (#603287, Sigma Aldrich) and euthanized 1 h later. About 30mg of tissues for each condition were first weighted and solubilized into 1.5 mL polypropylene microcentrifuge tubes, with 1 ml of cold lysate buffer (MeOH/Water/Chloroform, 9/1/1, -20°C). They were then homogenized three times for 20 s at 5500 rpm using Precellys 24 tissue homogenator (Bertin Technologies), followed by centrifugation (10min at 15000g, 4°C). Upper phase of the supernatant (600µl) was collected and evaporated in microcentrifuge tubes at 40°C in a pneumatically-assisted concentrator (Techne DB3). On dried extract, 300µl of methanol was added. Upper fraction of 150µl was collected and evaporated. The dried extract was solubilized with 300µl of MilliQ water, centrifugate (10min at 15000g 4°C) and aliquoted in 3 microcentrifuge tubes (100µl). Aliquots were transferred in UHPLC vials and injected into UHPLC/MS or kept at -80 °C until injection.

Sample preparation plasma (lithium heparin)

A volume of 50µl of plasma was mixed with a cold solvent mixture (MeOH/Water/Chloroform, 9/1/1, -20°C), into 1.5 mL polypropylene microcentrifuge tubes, vortexed and centrifugated (10min at 15000g, 4°C). On dried extract, 300µl of methanol was added. Upper fraction of 150µl was collected and evaporated. The dried extract was solubilized with 300µl of MilliQ water, centrifugate (10min at 15000g 4°C) and aliquoted in 3 microcentrifuge tubes (100µl). Aliquots were transferred in UHPLC vials and injected into UHPLC/MS or kept at -80 °C until injection.

Untargeted analysis of intracellular metabolites by ultra-high performance liquid chromatography (UHPLC) coupled to a quadrupole-time of flight (QTOF) mass spectrometer.

Profiling of intracellular metabolites was performed on a Liquid Chromatography (LC) 1260 system (Agilent Technologies) coupled to a QTOF 6520 (Agilent Technologies) equipped with an electrospray source operating in both positive and negative mode and full scan mode from 50 to 1000 Da. The gas temperature was set to 350°C with a gas flow of 12 l/min. The capillary voltage was set to 3.5 kV, and the fragmentor at 120 V. Two reference masses were used to maintain the mass accuracy during analysis: m/z 121.050873 and m/z 922.009798 in positive mode and m/z 112.985587 and m/z 980.016375 in negative mode.

10 µL of sample were injected on a SB-Aq column (100 mm × 2.1 mm particle size 1.8 µm) from Agilent Technologies, protected by a guard column XDB-C18 (5 mm × 2.1 mm particle size 1.8µm) and heated at 40°C.

The gradient mobile phase consisted of water with 0.2% of acetic acid (A) and acetonitrile (B). The flow rate was set to 0.3mL/min. Initial condition is 98% phase A and 2% phase B. Molecules were then eluted using a gradient from 2% to 95% phase B in 7min. The column was washed using 95% mobile phase B for 3 minutes and equilibrated using 2% mobile phase B for 3min.

The autosampler was kept at 4°C.

Data extraction

Profiles generated by LC-QTOF were processed using an in-house set of tools that convert raw MS data into a matrix compatible with statistical analysis. Raw data files were treated with the Molecular Feature Extraction (MFE) algorithm of the MassHunter Quantitative Analysis software, in order to identify predominant ions in form of triplets [mass to charge ratio (m/z); retention time (RT); intensity]. Ions (1) that were flagged as isotopes by the MFE algorithm, (2) that had a mass defect

between 0.75 and 0.95, (3) with a signal intensity below 3,500, and (4) outside the 0.8–10 min RT range were discarded. Those ions where further grouped and formed the basis to derived extract ion chromatograms (EICs) across all samples (tolerance: mass=16ppm, retention time=0.5 min) to ensure that peaks missed by the vendor MFE software and their isotopes with up to two 13C (tolerance: mass=20ppm) are entering peak deconvolution and integration. The final data tables are made with the characteristics (peak area, height, m/z, retention time) of the "potentially isotopically pure" precursors (labelled as M0) and those of their 2 potential isotopomers (labelled as M1/M2 at m/z+1.0033/2.0067 from M0). For each organ or biofluid, groups of M0/M1/M2 were excluded from downstream statistical analysis if they did not meet quality control (QC) criteria calculated from (1) the pooled QC samples and (2) samples from the control or unlabelled aspirin treated animals on the M0 feature.

Statistical analysis

 All statistical analyses and data representations were performed on pre-processed log2-transformed peak area. For differential analysis, moderated statistics (Ref I) were used and performed on the log2 (M0) features when comparing the effect of aspirin to the control samples (Asp/Co in the text) and on the log2(M1/M0) data matrices when comparing 13C labeled aspirin to its commercial/naturally labelled counterpart (^{13}C Asp /Asp in the text). For the latter, a large positive fold change (Log2FC in the text) demonstrates enrichment at +1.0033 m/z likely due to the 13C on the aspirin scaffold. Fold changes are reported without back-transformation alongside the associated p value. These are used to depict the heatmap on Figure 5G,H, the volcano plots and explicitly given in the **Table S2**.

C. elegans experiments.

Strains and genetics. We followed standard procedures for *C. elegans* strain maintenance (Brenner, 1974). Nematode rearing temperature was kept at 20°C. The following strains were used in this study: N2: wild-type Bristol isolate, DA2123: (*adIs2122*[p$_{lgg-1}$GFP::LGG-1 *rol-6(df)*], VK1093 (p$_{nhx-2}$mCherry::lgg-1), HZ589 (*him-5(e1490) V; bpIs151 [sqst-1p::sqst-1::GFP + unc-76(+)]*).

Plasmid construct and RNAi. For *cbp-1* RNAi experiment, we constructed a plasmid that directs the synthesis of a dsRNA corresponding to the *cbp-1* gene in *E. coli* bacteria, which were then fed to animals according to previously described methodology (Kamath et al., 2001).To construct the *cbp-1 RNAi* plasmid, a *cbp-1* gene-specific fragment was obtained by PCR amplification directly from *C.*

elegans genomic DNA using an appropriate pair of primers (5'-CTTGCCACCACCAGATATGC-3' and 5'-ATGAACCAGTGAAGCGATGC-3'). The PCR-generated fragment was subcloned into pCRII-TOPO vector (Invitrogen) from which it was excised as a *Pst*I/*Kpn*I fragment and inserted into the corresponding sites of the pL4440 plasmid vector. Engineering of the *bec-1*, *atg-7* and *dct-1* RNAi constructs was previously described. (Tasdemir et al., 2008) (Samara et al., 2008) (Palikaras et al., 2015) All the RNAi constructs were transformed into HT115(DE3) *E. coli* bacteria, deficient for RNase III (Kamath et al., 2001).

Autophagy assessment. Synchronous populations of GFP::LGG-1 expressing animals (Kang et al., 2007) were generated by hypochlorite treatment of gravid adults to obtain tightly synchronized embryos that were allowed to develop through the L4 larval stage on OP50 seeded plates. Animals were then transferred to plates containing aspirin or sodium salicylate (at the indicated concentrations) or equal volume of ethanol. Two- day old adults were treated for ∼ 5 min with a sodium hypochlorite solution. Freed embryos were collected and observed under a Zeiss Axio Imager Z2 Plus epifluorescence microscope equipped with a X40 objective lens (both from Carl Zeiss). To monitor autophagic activity in adults, nematodes expressing the SQST-1/p62::GFP and mCherry::LGG-1 transgenes were monitored on day 1 and day 2 of adulthood, as indicated. Worms were anaesthetized in 10mM sodium azide and observed using a Zeiss Axio Imager Z2 Plus Epifluorescence microscope. The number of GFP puncta in the pharyngeal region (SQST-1/p62::GFP) and mCherry puncta (mCherry::LGG-1) in the intestine were analyzed on grayscale images with a pixel depth of 8 bit (256 shades of grey) using the ImageJ software. To quantify GFP::LGG-1 upon knockdown of *cbp-1* or *dct-1*, 2-day-old adults were monitored using a Zeiss LSM 710 confocal microscope. Images were acquired with a X63 objective lens. For each animal, GFP puncta in the epidermis were counted in at least three separate regions of 208 μm^2 using *analyze particles* in ImageJ. Unless otherwise specified, all comparisons were performed using one-way ANOVA and unpaired *t*- test. For all microscopy experiments, more than 15 worms were scored in each experiment and all experiments were repeated at least twice.

Bafilomycin treatment was performed following the protocol of Pivtoraiko *et al.* (Pivtoraiko et al., 2010) with slight modifications. Wild-type animals expressing the GFP::LGG-1 reporter were transferred at the L4 molt to RNAi plates supplemented or not with aspirin (1mM) in the presence or absence of 100μg/ml bafilomycin A1 (LC Laboratories). Next day, young adults were allowed to lay

eggs for a limited time interval (4-5h), and then removed. Embryos were allowed to develop into L3 molt stage and then harvested for documentation as previously described.

Mitophagy measurements. Transgenic animals expressing mitochondria-targeted Rosella (mtRosella) biosensor in body wall muscle cells (Palikaras et al, 2015) were allowed to lay eggs on plates containing 1mM aspirin or equal volume of vehicle. Vehicle- and aspirin-treated animals were harvested at 3 day of adulthood and images were acquired using a X10 objective lens.

GFP-LC3 Immunoprecipitation. 5×10^6 HCT116 cells stably expressing a GFP-LC3 transgene were incubated for 16 hours with 5 mM sodium salicylate and for 6 hours with nutrient free medium respectively. At the end of the treatment cells were harvested and lysed in RIPA buffer and GFP-LC3 fusion protein was immunoprecipitated by means of GFP-Trap A system (#gt-250, Chromotek) as described by manufacturer. Total lysates and GFP immunoprecipitated was probed with an antibody recognizing GFP (to assess immunoprecipitation of GFP-LC3 tandem protein) and with an antibody specifically recognizing N-Acetylated protein residues. Levels of LC3 acetylation were normalized on GFP-immunoprecipitated signal.

Long-lived proteins degradation assay. HCT116 cells were incubated for 18 h at 37 °C with 0.2 µCi/mL-[14C] valine. Unincorporated radioisotope was removed by three rinses with phosphate-buffered saline (pH 7.4). Cells were then incubated in nutrient- and serum-free medium (without amino acids and in the absence of fetal calf serum) plus 0.1% bovine serum albumin and 10 mM unlabeled valine. When required, 10 mM 3-methyladenine (#M9281, Sigma Aldrich), a potent inhibitor of the formation of autophagic vacuoles, or $4 \times$ AA were added throughout the chase period. After the first hour of incubation, at which time short-lived proteins were being degraded, the medium was replaced with the appropriate fresh medium (in presence or absence of 5 mM sodium salicylate) and the incubation was continued for an additional 16 h period. Cells and radiolabeled proteins from the 16 h chase medium were precipitated in 10% (v/v) trichloroacetic acid at 4 °C. The precipitated proteins were separated from soluble radioactivity by centrifugation at $600 \times g$ for 10 min and then dissolved in 250 µl Soluene 350. The rate of protein degradation was calculated as acid-soluble radioactivity recovered from both cells and the medium.

Plasmids mutagenesis and transfection. Mutations in EP300 WT sequence were introduced by means of site-directed mutagenesis (#E0054, Q5® Site-Directed Mutagenesis Kit, New England Biolabs) using specifically designed primers. Transfection of EP300 WT plasmid and its mutated counterparts was performed using Fugene Transfection Reagent (#E2311, Promega).

Automated microscopy. Human U2OS osteosarcoma and HCT116 colorectal cancer cells stably expressing GFP-LC3 were seeded in 96-well or 384-wells imaging plates (BD Falcon, Sparks, USA) twenty-four h before stimulation to reach 70% confluence. Cells were treated with the indicated agents in absence or presence of the lysosomal inhibitor BafA1 (for the last two h of treatment) Subsequently, cells were fixed with 4% PFA and counterstained with 10 μM Hoechst 33342. Images were acquired using a BD pathway 855 automated microscope (BD Imaging Systems, San Jose, USA) equipped with a 40X objective (Olympus, Center Valley, USA) coupled to a robotized Twister II plate handler (Caliper Life Sciences, Hopkinton, USA). Images (5x5 frames), corresponding to 100-500 cells/well, were analyzed for the detection of GFP-LC3 puncta in the cytoplasm by means of the BD Attovision software (BD Imaging Systems). Cellular regions of interest, cytoplasm and nucleus, were defined and segmented according to standard procedures. RB 2x2 and Marr-Hildreth algorithms were employed to allow the detection of GFP LC3 puncta. Statistical analyses were conducted using Prism software.

Chemicals and culture conditions. Unless otherwise indicated, media and supplements for cell culture were purchased from Gibco-Thermo Fisher Scientific while plastic ware was purchased from Corning B.V. Life Sciences. Human osteosarcoma U2OS and their green fluorescent protein (GFP)-LC3-expressing derivatives (gift from Professor J. Yuan, Harvard University), were cultured in DMEM medium (#11965-092, Thermo Fisher Scientific) supplemented with 10% (v/v) fetal bovine serum (#10082139, Thermo Fisher Scientific), 100 mg/L sodium pyruvate (#11360070, Thermo Fisher Scientific) 10 mM HEPES buffer (#15630080, Thermo Fisher Scientific), 100 IU mL^{-1} penicillin G sodium salt, and 100 mg/mL streptomycin sulfate (#15140122, Thermo Fisher Scientific). Human colorectal cancer HCT116 wild type or EP300 knockout (purchased from Cancer Technology, upon MTA:008927) and their GFP-LC3-expressing derivatives were cultured in McCoy medium (#16600-082, Thermo Fisher Scientific) supplemented with 10% (v/v) fetal bovine serum, 100 mg/L sodium pyruvate, 10 mM HEPES buffer, 100 IU mL^{-1} penicillin G sodium salt, and 100 mg/mL streptomycin sulfate. Murine embryonic fibroblast (MEF) wild type cells and PRKAA α1/α2$^{-/-}$ (gift from Dr. B.

Viollet, Cochin Institut) were cultured in DMEM medium supplemented with 10% (v/v) fetal bovine serum, 100 mg/L sodium pyruvate, 10 mM HEPES buffer, 100 IU mL^{-1} penicillin G sodium salt, and 100 mg/mL streptomycin sulfate and 1 mM non-essential amino acids. All cells were maintained in standard culture conditions (at 37 ºC, under 5% CO2). Cells were seeded in 6-well, 96-wells or 384 well plates before treatment with 1.25 to 5 mM acetylsalicylic acid (#A5376, Sigma Aldrich) and sodium salicylate (#S3007, Sigma Aldrich), 10 µM C646 (#SML0002, Sigma Aldrich), 50 µM anacardic Acid (#A7236, Sigma Aldrich), 1.25 to 5 mM Ethyl-Salicylate (#112291, Sigma Aldrich), 100 nM bafilomycin A1 (#B1080, LC Laboratories), 1 µM Rapamycin (#R-5000, LC Laboratories).

Immunoblotting. For immunoblotting, protein extracts obtained by cellular lysis in radioimmunoprecipitation assay buffer (RIPA) buffer were run on 4-12% Bis-Tris acrylamide gels (#NP0322, Thermo Fisher Scientific) and electrotransferred to 0.2 µM polyvinylidene fluoride (PVDF) membranes (#1620177,Bio-Rad). Non-specific binding sites were saturated by incubating membranes for 1 h in 0.05% Tween 20 (#P9416, Sigma Aldrich) v:v in Tris-buffered saline (TBS) (#ET220, Euromedex) supplemented with 5% non-fat powdered milk (w:v in TBS), followed by an overnight incubation with primary antibodies specific for LC3B (#2775 Cell Signaling Technology), phospho-PRKAAα (Thr172) (#2531, Cell Signaling Technology), PRKAAα (#2532, Cell Signaling Technology), phospho-ACC (Ser79) (#3661, Cell Signaling Technology), ACC (#3662, Cell Signaling Technology), phospho-ribosomal protein S6 kinase (Thr389)(#9205, Cell Signaling Technology), ribosomal protein S6 kinase (#9202, Cell Signaling Technology), EP300 (N-15) (#sc-584,Santa-Cruz Biotechnology), SQSTM1/p62 (#H00008878-M0, Abnova), H3 (Lys56) (#4243, Cell Signaling Technology), H3 (#9715, Cell Signaling Technology), H2A (Lys5) (#2576, Cell Signaling Technology), H2A (#2578, Cell Signaling Technology), GFP (#2956, Cell Signaling Technology), Acetylated Lysine antibody (#9441, Cell Signaling). Membranes were cut in order to allow simultaneous detection of different molecular weight proteins. Equal protein loading was monitored by probing membranes with a glyceraldeyde-3-phosphate dehydrogenase (GAPDH)-specific antibody (#2118, Cell Signaling Technology). Membranes were developed with suitable horseradish peroxidase conjugates followed by chemiluminescence-based detection with the Amersham ECL Prime (#RPN2232, GE Healthcare and the ImageQuant LAS 4000 software-assisted imager (GE Healthcare, Piscataway, NJ, USA). Quantification was performed by densitometry by means of Image J software.

Autophagy was quantified through evaluation of LC3-II/GAPDH ratio and SQSTM1/GAPDH ratio according to (Klionsky et al., 2016). Posttranslational modifications (phosphorylation and acetylation) of specific residues were normalized on the levels of the respective total protein after membrane stripping (#21059, Thermo Fisher Scientific).

RNA interference in cell culture. Two different small interfering RNA (siRNA) sequences targeting EP300 (#6224, #6237; Sigma Aldrich) and PRKAA (#EHU074041 and #HA02727114, Sigma Aldrich) were reversed transfected by means of Lipofectamine RNAi MAX (#13778030, Thermo Fisher Scientific) transfection reagent.

Mouse experiments and tissue processing. For short-term autophagy induction studies, mice were treated with 100 mg/kg *i.p.* acetylsalicylic acid (Asp) 1 to 6 h after aspirin administration. To assess autophagic flux, 30 mg/kg *i.p.* leupeptin (SP-04-2217-A, Euromedex**)** was injected 2 hours before sacrifice. After treatment mice were euthanized and tissues were snap-frozen in liquid nitrogen after extraction and homogenized two cycles for 20 s at 5.500 rpm using a Precellys 24 tissue homogenator (Bertin Technologies) in 20 mM Tris buffer (pH 7.4) containing 150 mM NaCl, 1% Triton X-100, 10 mM EDTA and Complete® protease inhibitor cocktail (#000000011873580001, Sigma Aldrich). Tissue extracts were then centrifuged at 12,000 g at 4 ºC and supernatants were collected. Protein concentration in the supernatants was evaluated by the bicinchoninic acid technique (#23225, BCA protein assay kit). For cardiac mitophagy assessment, 2 months-old mito-Keima transgenic mice were treated for 2 weeks by oral gavage (five times a week) with aspirin (25 mg/kg), suspended in water. Fresh tissues were used for confocal microscopy studies. Heart tissues were rapidly taken out and rinsed with cold PBS. Thereafter, they were cut by a vibrating microtome within cold PBS into 10-15 sections (each 250µm). These sections were placed into a refrigerator (4°C) and immediately analyzed. Fluorescent samples were examined with a confocal microscope (Nikon Eclipse Ti). The excitation spectrum of the fluorescent probe mito-Keima varies according pH. While a short wavelength (457 nm) predominates at neutral pH, a longer (561 nm) wavelength prevails at low pH environment (corresponding to recruitment of mitochondria to lysosomes). Conditions of up regulated mitophagy are thus characterized by an elevated 561/457 ratio (quantified as mitophagy area).

For the evaluation of autophagic flux, 2-month-old Tg-tf-LC3 mice were treated for 2 weeks by oral gavage (five times a week) with aspirin (25 mg/kg), suspended in water. Chloroquine (#C6628, Sigma Aldrich) (10 mg/kg) was injected intraperitoneally 4 h before euthanasia. For in vivo determination of the number of fluorescent LC3 dots, fresh heart slices were embedded with tissue-TEK OCT compound (Sakura Fine technical Co., Ltd.) and frozen at -80 °C. 10-μm-thick sections were obtained from the frozen tissue samples by using a cryostat (CM3050S; Leica), air-dried for 30 min, fixed by 10% formalin for 10 min, mounted by using a reagent containing DAPI, and viewed under a fluorescence microscope.

Supplemental References

Brenner, S. (1974). The genetics of Caenorhabditis elegans. Genetics *77*, 71-94.

Kamath, R.S., Martinez-Campos, M., Zipperlen, P., Fraser, A.G., and Ahringer, J. (2001). Effectiveness of specific RNA-mediated interference through ingested double-stranded RNA in Caenorhabditis elegans. Genome Biol *2*, RESEARCH0002.

Kang, C., You, Y.J., and Avery, L. (2007). Dual roles of autophagy in the survival of Caenorhabditis elegans during starvation. Genes Dev *21*, 2161-2171.

Liu, X., Wang, L., Zhao, K., Thompson, P.R., Hwang, Y., Marmorstein, R., and Cole, P.A. (2008). The structural basis of protein acetylation by the p300/CBP transcriptional coactivator. Nature *451*, 846-850.

Palikaras, K., Lionaki, E., and Tavernarakis, N. (2015). Coordination of mitophagy and mitochondrial biogenesis during ageing in C. elegans. Nature *521*, 525-528.

Pivtoraiko, V.N., Harrington, A.J., Mader, B.J., Luker, A.M., Caldwell, G.A., Caldwell, K.A., Roth, K.A., and Shacka, J.J. (2010). Low-dose bafilomycin attenuates neuronal cell death associated with autophagy-lysosome pathway dysfunction. J Neurochem *114*, 1193-1204.

Samara, C., Syntichaki, P., and Tavernarakis, N. (2008). Autophagy is required for necrotic cell death in Caenorhabditis elegans. Cell Death Differ *15*, 105-112.

Tasdemir, E., Chiara Maiuri, M., Morselli, E., Criollo, A., D'Amelio, M., Djavaheri-Mergny, M., Cecconi, F., Tavernarakis, N., and Kroemer, G. (2008). A dual role of p53 in the control of autophagy. Autophagy *4*, 810-814.